play an important role as dipolar templates for the activation of substrate molecules. Of particular interest will be reactions with H_2 that may under certain conditions result in heterolytic cleavage of the H_2 bond and formation of the Mo(H)(O)(SH) hydride-hydrosulfide units. In general M(H)(SR) units are rather rare. Notable exceptions include the one present in the $[Mo(H)(tipt)_3(PMe_2Ph)_2]$ complex[48] (tipt = 2,4,6-$SC_6H_2(^iPr)_3$) and the Rh(H)(SR) units obtained by the *reversible* addition of H_2 into the Rh-S bonds of the $[(triphos)Ru(\mu\text{-}S)_2Rh(triphos)]^{2+}$ complex.[49] If the Mo(H)(O)(SH) units can be generated, they should be quite reactive, and some of their reactions with disulfides, thiophenes, and thiols may result in S-S or C-S bond cleavage with direct relevance to HDS catalysis.[19,21]

Acknowledgment. The support of this work by a grant from the National Science Foundation (CHE-90006069) is gratefully acknowledged. D.C. also acknowledges stimulating discussions with Prof. W. H. Pearson.

Supplementary Material Available: Tables S1-S3 containing listings of positional parameters, thermal parameters, and selected distances and angles of $[Ph_4P][(C_5H_5)Mo(O)(\mu\text{-}S)_2Mo(O)(S_2)]$, IV, $(Ph_4P)_2[(S_4)Mo(O)(\mu_2\text{-}S)_2Mo(O)(S)]$, IX, and $(Et_4N)_4\{[(S_4)Mo(O)(\mu_2\text{-}S)_2Mo(O)(S)]_2\}$, X (20 pages); Tables S4-S6 listing structure factors for IV, IX, and X (43 pages). Crystallographic data for the $[(DMF)_3Mo(O)(\mu\text{-}S)_2Mo(O)(S_2)]$ complex already has been deposited with a previous communication.[20] Ordering information is given on any current masthead page.

(46) Casewit, C. J.; Coons, D. E.; Wright, L. L.; Miller, W. K.; Rakowski DuBois, M. *Organometallics* **1986**, *5*, 951.
(47) Coons, D. E.; Laurie, J. C. V.; Haltiwanger, R. C.; Rakowski DuBois, M. *J. Am. Chem. Soc.* **1987**, *109*, 283.
(48) Burrow, T. E.; Lazarowych, N. J.; Morris, R. H.; Lane, J.; Richards, R. L. *Polyhedron* **1989**, *8*, 1701.
(49) (a) Bianchini, C.; Mealli, C.; Meli, A.; Sabat, M. *Inorg. Chem.* **1986**, *25*, 4617. (b) Bianchini, C.; Meli, A. *Inorg. Chem.* **1987**, *26*, 4268.

Cluster Core Isomerization from Planar to Tetrahedral: Experimental and Theoretical Aspects. Steric Control by the Ligands of Cluster Geometry. Synthesis and Crystal Structure of $[Pt_2Mo_2(\eta\text{-}C_5H_4CH_3)_2(CO)_6(PCy_3)_2]$

Pierre Braunstein,*,† Claude de Méric de Bellefon,† Salah-Eddine Bouaoud,‡ Daniel Grandjean,§ Jean-François Halet,§ and Jean-Yves Saillard*,§

Contribution from the Laboratoire de Chimie de Coordination, Associé au CNRS (UA 416), Université Louis Pasteur, F-67070 Strasbourg Cédex, France, Département de Chimie, Université de Constantine, Route de Ain-el-Bey, Constantine, Algérie, and Laboratoire de Cristallochimie, Associé au CNRS (UA 254), Université Rennes I, F-35042 Rennes Cédex, France.
Received May 8, 1990

Abstract: The reaction of the phosphine ligands PCy_3, $P(i\text{-}Pr)_3$, $PCyPh_2$, $P(m\text{-}Tol)_3$, $P(p\text{-}Tol)_3$ and $P(i\text{-}Bu)_3$, with the trinuclear complexes *trans*-$[Pt\{M(CO)_3Cp\}_2(PhCN)_2]$ (M = Mo, W; Cp = $\eta\text{-}C_5H_5$ or Cp′ = $\eta\text{-}C_5H_4CH_3$) affords the tetranuclear clusters $[Pt_2M_2Cp_2(CO)_6(PR_3)_2]$ (M = Mo, R_3 = Cy_3, **1**; M = Mo, R_3 = Cy_3, Cp = Cp′, **2**; M = W, R_3 = Cy_3, **3**; M = Mo, R_3 = $(i\text{-}Pr)_3$, **4**; M = W, R_3 = $(i\text{-}Pr)_3$, **5**; M = Mo, R_3 = $CyPh_2$, **6**; M = Mo, R_3 = $(m\text{-}Tol)_3$, **7**; M = Mo, R_3 = $(p\text{-}Tol)_3$, **8**; M = Mo, R_3 = $(i\text{-}Bu)_3$, **9**). Solution studies using ^{31}P NMR spectroscopy have revealed that clusters **1-5** exist as mixtures of two isomers. The geometry of the metallic skeleton is planar triangulated rhombohedral (PTR) in isomers **1a-5a**, like in clusters **6-9**, whereas it is tetrahedral in isomers **1b-5b**. The isomerization process was shown to be reversible, and its thermodynamics has been determined for some of these clusters. The solution ratio of the two structural isomers (i.e., b:a) depends on the solvent used, the temperature, and the steric and electronic properties of the phosphine ligand. Solvents such as toluene and bulky and basic phosphine ligands (e.g., PCy_3) favor the tetrahedral isomer b, whereas more polar solvents (e.g., dichloromethane) and small and/or less basic phosphine ligands (e.g., $P(p\text{-}Tol)_3$, $P(i\text{-}Bu)_3$) point to the planar isomer a. Crystal data for **2b**: monoclinic, space group $P2_1/n$ with $Z = 4$; $a = 10.321$ (3), $b = 24.351$ (8), $c = 21.368$ (6) Å; $\beta = 92.76$ (4)°; $V = 5364$ Å^3; $R = 0.042$, $R_w = 0.052$. Extended Hückel molecular orbital calculations have been carried out on the model compound $[Pt_2Mo_2Cp_2(CO)_6(PH_3)_2]$ in both PTR (a) and tetrahedral (b) geometries. The calculations have shown that, in isomer b, the Mo-Mo σ^* orbital is vacant and the Pt-Pt σ^* one is occupied, while in isomer a Mo-Mo σ^* is occupied and the LUMO has a strong Pt-Pt σ^* antibonding character. They confirmed the equilibrium measurements by revealing the existence of an avoided level crossing between isomers a and b, giving rise to an energy barrier and therefore to two isomers able to coexist in solution.

Introduction

Polyhedral rearrangement is one of the most challenging problems in cluster chemistry.[1] Possible mechanisms for the framework reorganization or isomerization of boranes or carboranes have been proposed already 20 years ago[2a] but are still under current investigation.[2b,c] The conditions for the tetrahedral → butterfly → square-planar transformations of the 20e X_2Y_2 Zintl ions have been recently investigated theoretically.[3] Being more recent, the chemistry of transition-metal clusters has provided only a few examples of *skeletal isomerism*.[4,5] This raises the question

† Laboratoire de Chimie de Coordination, Université Louis Pasteur.
‡ Département de Chimie, Université de Constantine.
§ Laboratoire de Cristallochimie, Université de Rennes I.

(1) For recent discussions, see: (a) Johnson, B. F. G. *J. Chem. Soc., Chem. Commun.* **1986**, 27. (b) Vahrenkamp, H. *Adv. Organomet. Chem.* **1983**, *22*, 169. (c) King, R. B. *Inorg. Chim. Acta* **1986**, *116*, 99. (d) King, R. B. In *Molecular Structures and Energetics*; Liebman, J. F., Greensberg, J. A., Eds.; Verlag Chemie: Deerfield Beach, FL, 1986; see also references cited therein. For a general review, see: Johnson, B. F. G. In *Transition Metal Clusters*; Johnson, B. F. G., Ed.; Wiley: London, 1980.
(2) (a) Lipscomb, W. N. *Science (Washington, D.C.)* **1966**, *153*, 373. (b) Gimarc, B. M.; Ott, J. J. *Inorg. Chem.* **1986**, *25*, 2708. (c) Wales, D. J.; Stone, A. J. *Inorg. Chem.* **1987**, *26*, 3845.

0002-7863/91/1513-5282$02.50/0

Scheme I

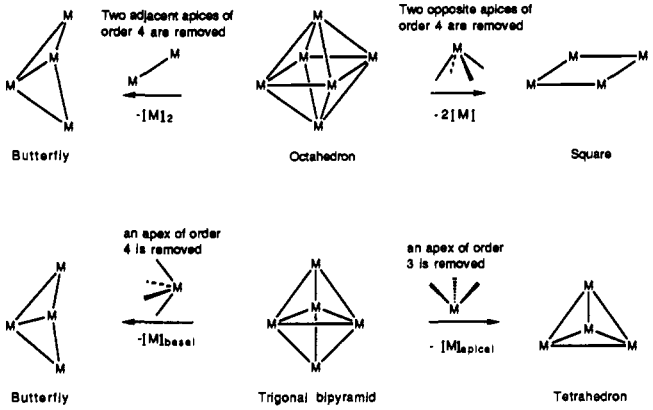

of the prediction of cluster skeleton geometries by using of the electron counting rules (ECR).[6] Thus, different electron counts for tetranuclear clusters will be in general easily related to their butterfly, square, or tetrahedral skeletal geometries. A butterfly geometry (with five metal–metal bonds) is generally considered as an arachno structure, derived from a closo octahedron by removal of two *adjacent* vertices[6c] and characterized by a total electron count (TEC) of 62 and the same number of skeletal electron pairs as the parent octahedron ($S = 7$). In principle, the square geometry can also be viewed as an octahedron-based arachno structure by removal of two *opposite* vertices. However, the TEC of such M_4 organometallic clusters is generally larger (e.g., 64 in $Os_4(CO)_{16}$).[7] The tetrahedral structure is usually considered as a nido structure derived from a trigonal bipyramid ($S = 6$), by removal of an *apical* vertex. The literal application of ECR indicates a TEC of 60 for the tetrahedron, as well as for the other nido butterfly derived from the trigonal bipyramid, by removal of an *equatorial* vertex (see Scheme I). We know from the published data that this is valid for the tetrahedral but not for the butterfly complexes, which generally bear 62e (Note that the angle between the wings of a butterfly derived from a regular trigonal bipyramid (141.0°) is different from the one of the butterfly derived from an octahedron (109.5°), but there is experimental evidence for the facile folding of butterfly skeletons[4b,5c]). These examples illustrate the importance of skeletal shape and metal to metal connectivity when considering the geometries derived from a parent polyhedron according to the electron counting rules. Deviations from these rules have been encountered when dealing with clusters differing in their electron count while keeping the same overall skeletal geometry, as in $[Ni_5(CO)_{12}]^{2-}$ which has a TEC of 76 instead of the expected one of 72.[8] These kinds of deviations have generally been rationalized by extended Hückel molecular orbital calculations.[9] Subtle changes in the π-acceptor properties of ligands (CO vs CH_2) have been invoked and substantiated by MO calculations to account for different geometries (butterfly and tetrahedral) for the isoelectronic 60e clusters $[PtOs_3(\mu\text{-}H)_2(CO)_{10}(PCy_3)(L)]$ (L = CO and CH_2, respectively).[10] The question we would like to address concerns a new class of isomeric clusters that also have the same electron count but exhibit different skeletal geometries. In other words, do the current electron counting rules account for cluster skeletal isomerism within a family of closely related molecules characterized by the same TEC?

As defined by Mingos in 1984, "skeletal isomers are compounds having the same stoichiometry but different skeletal geometries in the solid state",[5d] as encountered, e.g., in $[Pt_3(\mu\text{-}PPh_2)_3Ph(PPh_3)_2]$,[5h] $[Os_4S(CO)_{12}(HC_2Ph)]$,[11] $[ReAu_3H_2(PMe_2Ph)_3(PPh_3)_3]$,[12] $[Fe_4Au_2(CO)_{12}L_2BH]$ (L = phosphine),[5l] $[Ru_4Cu_2H_2(CO)_{12}\{P(i\text{-}Pr)_3\}_2]$,[13] $[Ru_6Au_2C(CO)_{16}(PEt_3)_2]$,[5f] $[Au_9\{P(C_6H_4OMe\text{-}p)_3\}_8][NO_3]_3$,[5d] or $[Os_{10}Au_nC(CO)_{24}(PR_3)_n]^{m-}$ (M = Cu, Ag, Au; $n = 1$, $m = 1$; $n = 2$, $m = 0$).[14] In these systems, each skeletal isomer has the same TEC as the other. In contrast, recent examples have been reported in which the change in geometry is accompanied by a change in the total electron count as in $[Fe_4(\mu\text{-}A)(CO)_{13}]^-$ (A = electrophilic fragment)[15] and $[WRu_3Cp(CO)_{12}H]$ (Cp = C_5H_5 or C_5Me_5).[16] Furthermore, clusters having the same skeletal geometry but that differ in the respective occupation of the vertices display an additional isomerism, a positional isomerism. This is particularly obvious when the atoms occupying the vertices are different in nature, as in $[FeRu_3N(CO)_{12}]^-$,[5e] $[Re_2Au_2H_6(PMe_2Ph)_4(PPh_3)_2]$,[17] $[Mo_2Fe_2S_2Cp_2(CO)_8]$,[5a,b,18] $[Hg\{Fe_2Rh\{\mu_3\text{-}COMe)(CO)_7Cp\}_2]$,[19] or $[FePdPt(CO)_4(\mu\text{-}dppm)_2]$.[5g,m] Note that, for these clusters, neither the overall geometry nor the electron count changes on going from one isomer to the other.

Clusters exhibiting reversible core isomerism are of considerable interest and should provide two characteristic pieces of information. The first concerns the activation energy (a kinetic factor), which reflects the ease with which the core rearrangement takes place and thus provides information about the mechanism. The second useful piece of information concerns the energy difference between the isomers (a thermodynamic factor), which reflects the energy cost of changing the geometry and/or the relative positions of the metal atoms. The determination of such data is of fundamental importance because one would like, eventually, to correlate them with the electron counting rules and help predict the dynamic behavior of the skeleton. Furthermore, such quantitative data are of obvious relevance to the dynamic phenomena occurring on metal alloy surfaces or particles.

(3) Cave, R. J.; Davidson, E. R.; Sautet, P.; Canadell, E.; Elsenstein, O. *J. Am. Chem. Soc.* **1989**, *111*, 8105.

(4) For a good introduction to isomerism in transition-metal clusters, see: (a) Müller, M.; Schacht, H.-T.; Fischer, K.; Ensling, J.; Gütlich, P.; Vahrenkamp, H. *Inorg. Chem.* **1986**, *25*, 4032. (b) Sappa, E.; Tiripicchio, A.; Carty, A. J.; Toogood, G. E. *Prog. Inorg. Chem.* **1987**, *35*, 437.

(5) For selected examples of cluster core isomerism, see: (a) Braunstein, P.; Jud, J.-M.; Tiripicchio, A.; Tiripicchio-Camellini, M.; Sappa, E. *Angew. Chem., Int. Ed. Engl.* **1982**, *21*, 307. (b) Williams, P. D.; Curtis, M. D.; Duffy, D. N.; Butler, W. M. *Organometallics* **1983**, *2*, 165. (c) Bruce, M. I.; Nicholson, B. K. *J. Organomet. Chem.* **1983**, *250*, 627. (d) Briant, C. E.; Hall, K. P.; Mingos, D. M. P. *J. Chem. Soc., Chem. Commun.* **1984**, 290. (e) Fjare, D. E.; Gladfelter, W. L. *J. Am. Chem. Soc.* **1984**, *106*, 4799. (f) Bunkhall, S. R.; Holden, H. D.; Johnson, B. F. G.; Lewis, J.; Pain, G. N.; Raithby, P. R.; Taylor, M. J. *J. Chem. Soc., Chem. Commun.* **1984**, 25. (g) Braunstein, P.; Kervennal, J.; Richert, J.-L. *Angew. Chem., Int. Ed. Engl.* **1985**, *24*, 768. (h) Bender, R.; Braunstein, P.; Tiripicchio, A.; Tiripicchio-Camellini, M. *Angew. Chem., Int. Ed. Engl.* **1985**, *24*, 861. (i) Lang, H.; Huttner, G.; Sigwarth, B.; Weber, U.; Zsolnai, L.; Jibril, I.; Orama, O. *Z. Naturforsh.* **1986**, *41B*, 191. (j) Huttner, G.; Knoll, K. *Angew. Chem., Int. Ed. Engl.* **1987**, *26*, 743. (k) Wucherer, E. J.; Tasi, M.; Hansert, B.; Powell, A. K.; Garland, M. T.; Halet, J.-F.; Saillard, J.-Y.; Vahrenkamp, H. *Inorg. Chem.* **1989**, *28*, 3564. (l) Housecroft, C. E.; Shongwe, M. S.; Rheingold, A. L. *Organometallics* **1989**, *8*, 2651. (m) Braunstein, P.; Richert, J.-L.; Dusausoy, Y. *J. Chem. Soc., Dalton Trans.* **1990**, 3801.

(6) (a) Wade, K. *Adv. Inorg. Chem. Radiochem.* **1976**, *18*, 1. (b) Lauher, J. W. *J. Am. Chem. Soc.* **1975**, *97*, 5034. (c) Mingos, D. M. P. *Acc. Chem. Res.* **1984**, *17*, 311.

(7) (a) Johnston, V. J.; Einstein, F. W. B.; Pomeroy, R. K. *J. Am. Chem. Soc.* **1987**, *109*, 8111. (b) Lauher, J. W. *Int. J. Quantum Chem.* **1988**, *22*, 309.

(8) Longoni, G.; Chini, P.; Lower, L. D.; Dahl, L. F. *J. Am. Chem. Soc.* **1975**, *97*, 5034.

(9) Johnston, R. L.; Mingos, D. M. P. *J. Chem. Soc., Dalton Trans.* **1987**, 647.

(10) (a) Ewing, P.; Farrugia, L. J. *New J. Chem.* **1988**, *12*, 409. (b) Ewing, P.; Farrugia, L. J. *Organometallics* **1989**, *8*, 1665.

(11) Adams, R. D.; Wang, S. *J. Am. Chem. Soc.* **1987**, *109*, 924.

(12) Sutherland, B. R.; Folting, K.; Streib, W. E.; Ho, D. M.; Huffman, J. C.; Caulton, K. G. *J. Am. Chem. Soc.* **1987**, *109*, 3489.

(13) Adatia, T.; McCarthy, P. J.; McPartlin, M.; Rizza, M.; Salter, I. D. *J. Chem. Soc., Chem. Commun.* **1988**, 1106.

(14) Drake, S. R.; Johnson, B. F. G.; Lewis, J. *J. Organomet. Chem.* **1988**, *340*, C31.

(15) (a) Horwitz, C. P.; Holt, E. M.; Brock, C. P.; Shriver, D. F. *J. Am. Chem. Soc.* **1985**, *107*, 8136. (b) Horwitz, C. P.; Shriver, D. F. *J. Am. Chem. Soc.* **1985**, *107*, 8147. (c) Wang, J.; Sabat, M.; Horwitz, C. P.; Shriver, D. F. *Inorg. Chem.* **1988**, *27*, 552.

(16) Chi, Y.; Wu, F.-J.; Liu, B.-J.; Wang, C.-C.; Wang, S.-L. *J. Chem. Soc., Chem. Commun.* **1989**, 873.

(17) Sutherland, B. R.; Ho, D. M.; Huffman, J. C.; Caulton, K. G. *Angew. Chem., Int. Ed. Engl.* **1987**, *26*, 135.

(18) Bogan, L. E., Jr.; Rauchfuss, T. B.; Rheingold, A. L. *J. Am. Chem. Soc.* **1985**, *107*, 3843.

(19) Farrugia, L. J. *J. Chem. Soc., Chem. Commun.* **1987**, 147.

Table I. $^{31}P\{^1H\}$ NMR Data[a]

planar isomers		δ	^3J(PP)	^1J(PtP)	^2J(PtP)	^1J(PtPt)
$[Pt_2Mo_2Cp_2(CO)_6(PCy_3)_2]$[b]	(1a)	53.3	102	4372	-96	
$[Pt_2Mo_2Cp'_2(CO)_6(PCy_3)_2]$	(2a)	52.3	101.5	4416	-99	
$[Pt_2W_2Cp_2(CO)_6(PCy_3)_2]$[b]	(3a)	54.4	98.5	4436	-98	913
$[Pt_2Mo_2Cp_2(CO)_6\{P(i\text{-}Pr)_3\}_2]$	(4a)	63.6	102	4364	-97	720
$[Pt_2W_2Cp_2(CO)_6\{P(i\text{-}Pr)_3\}_2]$	(5a)	64.5	99	4423	-99	949
$[Pt_2Mo_2Cp_2(CO)_6(PCyPh_2)_2]$	(6)	50.3	111	4436	-107	707
$[Pt_2Mo_2Cp_2(CO)_6\{P(m\text{-}Tol)_3\}_2]$	(7)	46.4	108	4615	-110	738
$[Pt_2Mo_2Cp_2(CO)_6\{P(p\text{-}Tol)_3\}_2]$[c]	(8)	47.1	107.5	4617	-111	745
$[Pt_2Mo_2Cp_2(CO)_6\{P(i\text{-}Bu)_3\}_2]$[b]	(9)	31.0	93	4379	-102	763
tetrahedral isomers		**δ**	**^3J(PP)**	**^1J(PtP)**	**^2J(PtP)**	**^1J(PtPt)**
$[Pt_2Mo_2Cp_2(CO)_6(PCy_3)_2]$	(1b)	42.5	11	4855	186.5	1998
$[Pt_2Mo_2Cp'_2(CO)_6(PCy_3)_2]$	(2b)	42.4	10.5	4942	190	
$[Pt_2W_2Cp_2(CO)_6(PCy_3)_2]$[b]	(3b)	57.2	7.5	4796	193	1977
$[Pt_2Mo_2Cp_2(CO)_6\{P(i\text{-}Pr)_3\}_2]$	(4b)	53.5	11	4895	185.5	1946
$[Pt_2W_2Cp_2(CO)_6\{P(i\text{-}Pr)_3\}_2]$	(5b)	68.6	6	4840	193	1920

[a] Chemical shifts δ (ppm), coupling constants J (Hz); spectra measured in $CDCl_3$ unless otherwise stated. [b] In $CDCl_3/CH_2Cl_2$. [c] In CD_2Cl_2.

Following the first example of skeletal isomerism in transition-metal cluster chemistry with $[Au_9\{P(C_6H_4OMe\text{-}p)_3\}_8][NO_3]_3$ [5d] and the increasing, but still small, number of papers dealing with metal core isomerism,[4,5,11-19] we wish to describe here our own results concerning this topic. Thus, we report in this paper (i) on the reactions of the readily available chain complex *trans*-$[Pt\{M(CO)_3Cp\}_2(PhCN)_2]$ (M = Mo, W; Cp = Cp or Cp') with phosphine ligands ($P(o\text{-}Tol)_3$, PCy_3, $P(i\text{-}Pr)_3$, $P(m\text{-}Tol)_3$, $PCyPh_2$), $P(p\text{-}Tol)_3$, and $P(i\text{-}Bu)_3$ whose cone angles range from 194 to 143°[20]), which lead to new tetranuclear Pt_2Mo_2 and Pt_2W_2 clusters; (ii) on the demonstration that steric hindrance is responsible for the folding of the tetranuclear cores of these clusters from a planar to a tetrahedral geometry; (iii) on the existence in solution of interconvertible isomeric clusters; (iv) on the X-ray characterization of the tetranuclear cluster $[Pt_2Mo_2(\eta\text{-}C_5H_4CH_3)_2(CO)_6(PCy_3)_2]$ (**2b**); and finally (v) on a molecular orbital analysis of the planar and tetrahedral structures for this family of clusters.

Results

Synthesis. The reaction of the trinuclear complex *trans*-$[Pt\{Mo(CO)_3Cp\}_2(PhCN)_2]$ (Cp = η-C_5H_5) with 1 equiv of PCy_3 (Cy = c-C_6H_{11}) in refluxing tetrahydrofuran (THF) affords the new heterometallic complexes $[Pt_2Mo_2Cp_2(CO)_6(PCy_3)_2]$ (**1**) (48%) and $[PtCl\{MoCp(CO)_3\}(CO)(PCy_3)]$ (ca. 5%)[21] and $[Mo(CO)_3Cp]_2$ (34%)[22] and $[Pt_3(\mu\text{-}CO)_3(PCy_3)_3]$ (4%),[23] which were separated by column chromatography (eq 1).

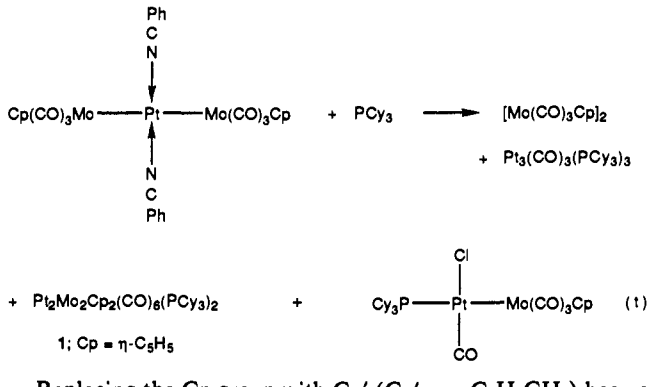

Replacing the Cp group with Cp' (Cp' = η-$C_5H_4CH_3$) has no influence on either the product distribution or the yields. However, the use of Cp instead of Cp' facilitates the isolation of pure **1** by chromatography, whereas $[Pt_2Mo_2Cp'_2(CO)_6(PCy_3)_2]$ (**2**) remains contaminated with $[PtCl\{MoCp'(CO)_3\}(CO)(PCy_3)]$[21] under the same conditions (see Experimental Section). That the Mo_2 dimer, the trinuclear Pt_3, and the tetranuclear Pt_2Mo_2 clusters are all formed is consistent with a redox mechanism, probably involving radical intermediates, as already proposed for the formation of the closely related clusters $[M'_2M_2Cp_2(CO)_6(PR_3)_2]$ (M' = Pt, Pd; M = Cr, Mo, W; R = Me, Et, *n*-Bu, Ph).[24]

When *trans*-$[Pt\{M(CO)_3Cp\}_2(PhCN)_2]$ (M = Mo, W) was reacted with $P(i\text{-}Pr)_3$, $PCyPh_2$, $P(m\text{-}Tol)_3$, $P(p\text{-}Tol)_3$, or $P(i\text{-}Bu)_3$, the only isolated products were $[M(CO)_3Cp]_2$ (M = Mo, W) and the tetranuclear clusters $[Pt_2M_2Cp_2(CO)_6(PR_3)_2]$ (M = W, R_3 = Cy_3, **3**; M = Mo, R_3 = $(i\text{-}Pr)_3$, **4**; M = W, R_3 = $(i\text{-}Pr)_3$, **5**; M = Mo, R_3 = $CyPh_2$, **6**; M = Mo, R_3 = $(m\text{-}Tol)_3$, **7**; M = Mo, R_3 = $(p\text{-}Tol)_3$, **8**; M = Mo, R_3 = $(i\text{-}Bu)_3$, **9**). However, with *trans*-$[Pt\{Mo(CO)_3Cp\}_2(PhCN)_2]$ and $P(o\text{-}Tol)_3$, only decomposition occurred, yielding platinum metal and $[Mo(CO)_3Cp]_2$ (as evidenced by IR and $^{31}P\{^1H\}$ NMR spectroscopies).[22,25]

It is noteworthy that the clusters containing trialkyl phosphines (i.e., **1**–**5** and **9**) are more soluble than their analogues with triaryl- and diarylalkylphosphines (i.e., **6**, **7**, and **8**). This allows the use of chromatographic separation for the former, yielding red-brown microcrystalline powders, whereas the latter clusters are obtained as pure dark green microcrystals after recrystallization from CH_2Cl_2/*n*-hexane. Interestingly, when cluster **1** was recrystallized slowly from CH_2Cl_2/*n*-hexane, dark green, well-shaped crystals formed. They provided the same analytical results as red-brown **1**.

Spectroscopic Characterization. The analytical and IR data of these tetranuclear Pt_2M_2 clusters are consistent with their belonging to the family of structurally fully characterized and closely related clusters $[M'_2M_2Cp_2(CO)_6(PR_3)_2]$ (M' = Pt, Pd; M = Cr, Mo, W; R = Me, Et, *n*-Bu, Ph).[24] Thus, the ν(CO) frequencies found between 1728 and 1802 cm^{-1} are typical for only bridging carbonyl ligands being present.

The $^{31}P\{^1H\}$ NMR spectra clearly indicate the presence of a P–Pt–Pt–P arrangement, which is characterized by the superimposition of the spectra of the three isotopomers (relative abundance) P–Pt–Pt–P (44%), P–^{195}Pt–Pt–P (44.7%), and P–^{195}Pt–^{195}Pt–P (11.3%). Such systems have been analyzed previously.[24b] The $^{31}P\{^1H\}$ NMR data for clusters **6**–**9** agree well with the planar triangulated rhombohedral (PTR) structures previously encountered in clusters $[Pt_2Mo_2(Cp)_2(CO)_6(PR_3)_2]$ (R = Me, Et, *n*-Bu). Indeed, these Pt_2Mo_2 clusters possess typical ^1J(PtP), ^2J(PtP), and ^3J(PP) coupling constants in the range of 4350 to 4620, –96 to –111, and 91 to 107.5 Hz, respectively (see Table I). In contrast, the spectra of complexes **1**–**5** reveal a mixture of two

(20) Tolman, C. A. *Chem. Rev.* **1977**, *77*, 313.
(21) The chloride ligand in this heterodinuclear complex originates from the solvent (de Méric de Bellefon, C. Thèse de 3ème Cycle. Université Louis Pasteur, Strasbourg, 1985).
(22) Fischer, R. D.; Noack, K. *J. Organomet. Chem.* **1969**, *16*, 125.
(23) (a) Albinati, A. *Inorg. Chim. Acta* **1977**, *22*, L31. (b) Moor, A.; Pregosin, P. S.; Venanzi, L. M. *Inorg. Chim. Acta* **1981**, *48*, 153.
(24) (a) Bender, R.; Braunstein, P.; Jud, J.-M.; Dusausoy, Y. *Inorg. Chem.* **1983**, *22*, 3394. (b) Bender, R.; Braunstein, P.; Jud, J.-M.; Dusausoy, Y. *Inorg. Chem.* **1984**, *23*, 4489.
(25) Pinnell, R. P.; Megerle, C. A.; Manatt, S. L.; Kroon, P. A. *J. Am. Chem. Soc.* **1973**, *95*, 977.

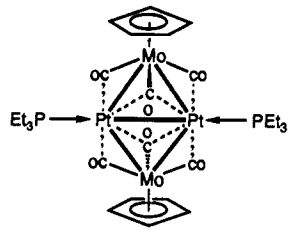

The planar triangulated rhombohedral (PTR) structure

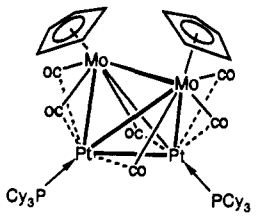

The tetrahedral structure

spectroscopically different compounds a and b, each having a P–Pt–Pt–P arrangement. The coupling constants and chemical shifts are in the expected range (^1J(PtP) ca. 4000 Hz). One family of clusters (i.e., **1a–5a**) possesses a PTR core structure (^2J(PtP) and ^3J(PP) criterion), whereas the other (**1b–5b**) should have a different geometry, since it presents a positive ^2J(PtP) (185–190 Hz) and a surprisingly small ^3J(PP) coupling (ca. 10 Hz). The ^{1}H NMR spectra of **1–5** also confirm the presence of two forms in solution, although the signals for isomers a and b sometimes overlap, precluding a definitive attribution.

The situation is different with phosphines having a cone angle smaller than that of P(*i*-Pr)$_3$ (165°): Only the planar form a is observed for the trialkylphosphines PMe$_3$ and P(*n*-Bu)$_3$ (cone angle <132°) and for the triaryl- or aryldiarylphosphines PCyPh$_2$, P(*p*-Tol)$_3$, and P(*m*-Tol)$_3$ (between 145 and 153°).[20] In order to establish unambiguously the geometry of form b, an X-ray diffraction study was performed on cluster **2b** (see below).

Crystal Structure of [Pt$_2$Mo$_2$(η-C$_5$H$_4$CH$_3$)$_2$(CO)$_6$(PCy$_3$)$_2$] (2b). The molecular geometry of cluster **2b** was fully determined by a single-crystal X-ray analysis. The structure consists of discrete molecules of **2b**, two molecules in the unit cell, and no abnormally short intermolecular contacts. Interatomic distances and angles are collected in Table II and III, respectively. Figure 1 shows an ORTEP plot of a molecule of **2b** with the atom numbering scheme. The metal core of **2b** may be viewed as a distorted tetrahedron with two longer edges (Mo–Mo = 3.126 (1) Å and Pt–Pt = 2.992 (1) Å) or as a butterfly if one prefers to consider the Mo–Mo distance as corresponding to a nonbonding separation (see Discussion and Figure 1). Each wing of the butterfly consists of a nonregular PtMo$_2$ triangle. Thus, the Pt(1)–Mo(1) bond is significantly shorter (0.115 Å) than the Pt(2)–Mo(1) bond. The Pt(1)Mo(2)Pt(2) triangle is more distorted, with the Pt(2)–Mo(2) bond being 0.157 Å shorter than the Pt(1)–Mo(2) bond. All the Pt–Mo distances compare well with those previously reported for such a bond in heterometallic clusters.[24b] The dihedral angle between the two wings of the butterfly (Pt(1)Mo(1)Pt(2) and Pt(1)Mo(2)Pt(2) planes) is 82°, and that between the planes Mo(1)Pt(1)Mo(2) and Mo(1)Pt(2)Mo(2) is 79.5°.

Among the six carbonyl ligands, four bridge symmetrically the Pt–Mo edges (i.e., C(49)O(1), C(51)O(3), C(53)O(5), C(54)O(6)). The other two (C(50)O(2) and C(52)O(4)) unsymmetrically bridge the Pt(2)–Mo(2) and Pt(1)–Mo(1) edges, respectively. The coordination geometry about the molybdenum atoms is very similar. It is of the strongly distorted three-legged piano stool type with the CpMo(CO)$_3$ fragment bridging the Pt(1)–Pt(2) bond. Instead of the more symmetrical situation encountered in the related clusters [Pt$_2$Mo$_2$Cp$_2$(CO)$_6$PEt$_3$)$_2$], where the (OC)–Mo–(CO) angles between adjacent carbonyls range from 94 (1) to 112 (1)° (molecule A) or from 86 (1) to 114 (1)° (molecule B), the corresponding limits about Mo(1) in **2b** are found for C(53)–Mo(1)–C(54) and C(52)–Mo(1)–C(54), with angles of 75.3 (3) and 141.6 (4)°, respectively. This reflects the fact that C(52)O(4) is semibridging the Mo(1)–Pt(1) edge and not the Pt$_2$Mo(1) face, as in the rigorously planar [Pt$_2$Mo$_2$Cp$_2$-(CO)$_6$(PEt$_3$)$_2$] cluster. Similarly, the angles between adjacent carbonyls at Mo(2) range between 71.5 (3) and 143.4 (4)°.

Viewing the coordination about Mo(1) or Mo(2) as being of the four-legged piano stool type represents an attractive alternative, as the other Mo atom occupies almost ideally the fourth position, with the Mo(1)Mo(2) distance of 3.126 (1) Å being shorter than

Table II. Selected Interatomic Distances in **2b**

bond[a]	bond length (Å)[b]	bond[a]	bond length (Å)[b]
Pt(1)–Pt(2)	2.992 (1)	Mo(1)–Mo(2)	3.126 (1)
Pt(1)–Mo(1)	2.755 (1)	Mo(1)–C(50)	2.76 (1)
Pt(1)–Mo(2)	2.884 (1)	Mo(1)–C(52)	2.02 (1)
Pt(2)–Mo(1)	2.870 (1)	Mo(1)–C(53)	1.997 (8)
Pt(2)–Mo(2)	2.727 (1)	Mo(1)–C(54)	2.342 (9)
Pt(1)–P(1)	2.299 (2)	Mo(1)–Cp [C(43)–C(47)]	1.99 (2)
Pt(2)–P(2)	2.291 (2)	Mo(2)–C(49)	2.022 (9)
Pt(1)–C(51)	1.97 (1)	Mo(2)–C(50)	2.00 (1)
Pt(1)–C(52)	2.53 (1)	Mo(2)–C(51)	2.42 (1)
Pt(1)–C(53)	2.225 (9)	Mo(2)–C(52)	2.70 (1)
Pt(2)–C(49)	2.183 (9)	Mo(2)–Cp [C(37)–C(41)]	1.98 (2)
Pt(2)–C(50)	2.50 (1)		
Pt(2)–C(54)	1.939 (9)		

[a] Atoms are labeled in agreement with Figure 1. [b] Numbers in parentheses are estimated standard deviations in the least significant digit.

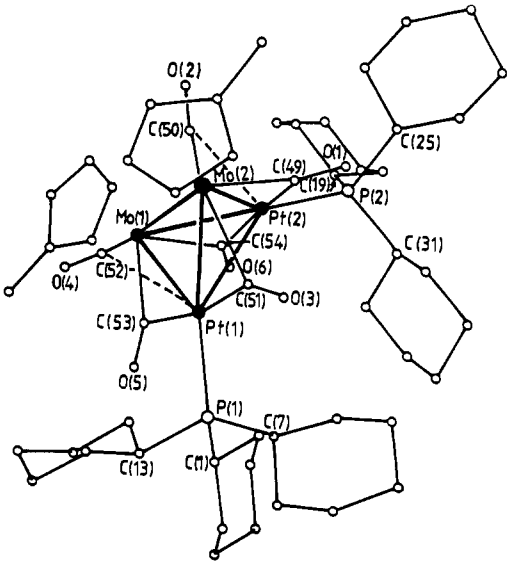

a

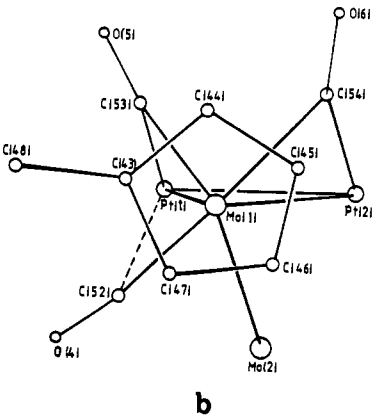

b

Figure 1. (a) View of the molecular structure of cluster [Pt$_2$Mo$_2$Cp$'_2$-(CO)$_6$(PCy$_3$)$_2$] (**2b**), illustrating the numbering scheme. (b) View through the C(43)–C(47) ring, showing the four-legged piano stool type environment around Mo(1).

in the dimers [CpMo(CO)$_3$]$_2$ (3.235 (1) Å) and [(η-C$_5$Me$_5$)-Mo(CO)$_3$]$_2$ (3.278 (4) Å) and in [Cp(η-C$_7$H$_7$)Mo$_2$(CO)$_5$] (3.160 (1) Å).[26] Angles between adjacent ligands of 77–78° are usually found for four-legged piano stool arrangements, i.e., for compounds containing the η^1-MoCp(CO)$_3$ fragment.[27]

(26) (a) Adams, R. D.; Collins, D. M.; Cotton, F. A. *Inorg. Chem.* **1974**, *13*, 1086. (b) Leoni, P.; Marchetti, F.; Pasquali, M.; Zanello, P. *J. Chem. Soc., Dalton Trans.* **1988**, 635. (c) Beddoes, R. L.; Ricalton, A.; Whiteley, M. W. *Acta Crystallogr. C* **1988**, *44*, 2025.

Table III. Selected Interatomic Bond Angles in 2b

bond[a]	bond angles (deg)[b]	bond[a]	bond angles (deg)[b]
Metallic Framework			
Pt(1)-Pt(2)-Mo(1)	56.02 (2)	Pt(2)-Mo(2)-Mo(1)	58.25 (2)
Pt(1)-Pt(2)-Mo(2)	60.35 (2)	Mo(1)-Pt(1)-Mo(2)	67.29 (2)
Pt(1)-Mo(1)-Pt(2)	64.24 (2)	Mo(1)-Pt(2)-Mo(2)	67.87 (2)
Pt(1)-Mo(1)-Mo(2)	58.31 (2)	Pt(1)-Pt(2)-P(2)	138.73 (5)
Pt(1)-Mo(2)-Pt(2)	64.39 (2)	Pt(2)-Pt(1)-P(1)	140.07 (5)
Pt(1)-Mo(2)-Mo(1)	54.40 (2)	Mo(1)-Pt(1)-P(1)	140.36 (6)
Pt(2)-Pt(1)-Mo(1)	59.74 (2)	Mo(1)-Pt(2)-P(2)	148.40 (6)
Pt(2)-Pt(1)-Mo(2)	55.26 (2)	Mo(2)-Pt(1)-P(1)	149.87 (6)
Pt(2)-Mo(1)-Mo(2)	53.89 (2)	Mo(2)-Pt(2)-P(2)	141.58 (6)
Metal-Carbonyl Angles			
Pt(1)-C(51)-O(3)	148.8 (7)	Mo(1)-C(52)-O(4)	157 (1)
Pt(1)-C(52)-O(4)	120.4 (7)	Mo(1)-C(53)-O(5)	149.8 (7)
Pt(1)-C(53)-O(5)	128.9 (7)	Mo(1)-C(54)-O(6)	131.2 (7)
Pt(2)-C(49)-O(1)	133.5 (7)	Mo(2)-C(49)-O(1)	145.8 (8)
Pt(2)-C(50)-O(2)	120.3 (7)	Mo(2)-C(50)-O(2)	158.6 (8)
Pt(2)-C(54)-O(6)	145.0 (7)	Mo(2)-C(51)-O(3)	129.7 (6)
Mo(1)-C(50)-O(2)	119.3 (7)	Mo(2)-C(52)-O(4)	119.6 (7)
Carbonyl Coordination around Mo(1)			
C(50)-Mo(1)-C(52)	88.1 (4)	C(52)-Mo(1)-C(53)	87.2 (4)
C(50)-Mo(1)-C(53)	144.0 (3)	C(52)-Mo(1)-C(54)	141.6 (4)
C(50)-Mo(1)-C(54)	86.6 (4)	C(53)-Mo(1)-C(54)	75.3 (3)
Carbonyl Coordination around Mo(2)			
C(49)-Mo(2)-C(50)	89.1 (4)	C(50)-Mo(2)-C(51)	143.4 (4)
C(49)-Mo(2)-C(51)	71.5 (3)	C(50)-Mo(2)-C(53)	90.2 (3)
C(49)-Mo(2)-C(52)	141.7 (2)	C(51)-Mo(2)-C(53)	87.1 (3)

[a] Atoms are labeled in agreement with Figure 1. [b] Numbers in parentheses are estimated standard deviations in the least significant digit.

Table IV. Equilibrium Data of the Planar to Tetrahedral Core Isomerization for the Clusters $[Pt_2M_2Cp_2(CO)_6(PR_3)_2]$

compounds			K_{eq} = [b]/[a][a]			$\Delta H°$	$\Delta S°$
M	PR_3		CH_2Cl_2	$CHCl_3$	toluene	(kJ·mol^{-1})	(J·K^{-1}·mol^{-1})
W	PCy_3	3	0.6	2.2		7.3 ± 0.4[b]	20.1 ± 1.5[b]
Mo	$P(i\text{-}Pr)_3$	4	1.4	1.6	2.6	6.0 ± 0.3[b]	22.4 ± 1.2[b]
W	$P(i\text{-}Pr)_3$	5	0.18	0.52	1.6	16.4 ± 1.4[c]	42 ± 5[c]

[a] At room temperature. [b] Measured in dichloromethane. [c] Measured in chloroform.

The two tricyclohexylphosphine ligands are cisoid with respect to the Pt(1)-Pt(2) segment with the P(1)Pt(1)Pt(2) and P(2)-Pt(2)Pt(1) angles of 140.07 (5) and 138.73 (5)°, respectively. The two methylcyclopentadienyl groups present normal carbon-molybdenum bond distances. Each ring is located at the top of each wing in such a way that the Cp'(1) and Cp'(2) rings are almost orthogonal to the Pt(1)Mo(1)Pt(2) and Pt(1)Mo(2)Pt(2) triangles, respectively (82.1 and 79.1°).

NMR Analysis of the Interconversion between Forms a and b. We have investigated in detail the solution behavior of isomers a and b. Their solution ratio (i.e., b:a) depends on the solvent used, the temperature, and the steric and electronic properties of the phosphine ligand. Thus, solvents having a small dielectric constant (e.g., toluene) and bulky and basic phosphine ligands (e.g., PCy_3) favor the tetrahedral isomer b, whereas more polar solvents (e.g., dichloromethane) and small and/or less basic phosphine ligands (e.g., $P(p\text{-Tol})_3$, $P(i\text{-Bu})_3$) lead to the planar isomer a (Table IV).

In a typical experiment, the cluster (3, 4, and 5; 0.06–0.10 g) was dissolved in the appropriate solvent (ca. 2 mL of CD_2Cl_2, $CDCl_3$, or toluene-d_8) and sampled in a 10-mm NMR tube. The $^{31}P\{^1H\}$ NMR spectra were recorded and the ratio K_{eq} = [b]/[a] was determined by peak integration of the main phosphorus resonances (i.e., the A_2 subspectra; see above). Values of $\Delta H°$ and $\Delta S°$ for the tetrahedron (b) to butterfly (a) isomerization for clusters 3, 4, and 5 were calculated from the slope and intercept of the least-squares line and fit to more than seven data points for each compound[28] (Figure 2). In order to see whether the equilibrium was rapidly reached, crystalline samples of 4 or 5 (because of higher solubility) were dissolved at room temperature and then either slowly (ca. 2 h) or rapidly (ca. 0.2 h) cooled to the temperature of the NMR experiment (203 K) or their solution maintained in an external low-temperature bath for 24 h. The b:a ratios observed under these different conditions were identical (within experimental error), showing that, upon dissolution of the solid, rapid (on the chemical time scale) equilibration between the isomers occurred. Dissolution of the crystals of, e.g., 4 at ca. 204 K was too slow to allow recording of the spectrum under these conditions.

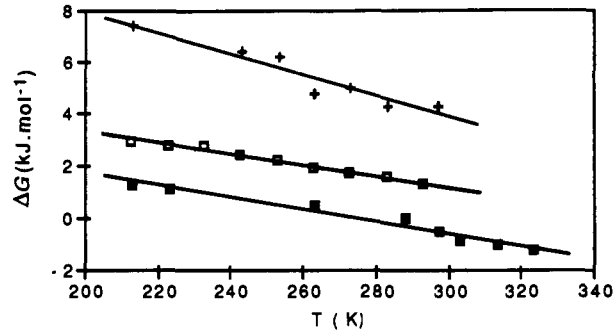

Figure 2. Equilibrium data for the planar to tetrahedral core isomerization of (a) $[Pt_2W_2Cp_2(CO)_6(PCy_3)_2]$ (3) (□), (b) $[Pt_2Mo_2Cp_2(CO)_6\{P(i\text{-}Pr)_3\}_2]$ (4) (■) in CH_2Cl_2/CD_2Cl_2, and (c) $[Pt_2W_2Cp_2(CO)_6\{P(i\text{-}Pr)_3\}_2]$ (5) (+) in $CDCl_3$.

Discussion

Discussion of the Synthesis and Isomerization. The synthesis of mixed-metal clusters may be achieved by using appropriate mononuclear complexes or preformed heterometallic precursors. We have shown that platinum-group six mixed-metal chain complexes of the type *trans*-$[Pt\{M(CO)_3Cp\}_2(PhCN)_2]$ (M = Cr, Mo, W) are excellent precursors for the high-yield synthesis of the planar, triangulated heterotetranuclear clusters $[Pt_2M_2Cp_2(CO)_6(PR_3)_2]$ (R = Me, Et, *n*-Bu, Ph). The reaction proceeds first by replacement of the labile benzonitrile ligands with the desired phosphine ligands, followed by metal-metal bond rupture and cluster formation.[24b] With the diphosphine ligand $Ph_2PCH_2CH_2PPh_2$ (dppe), the metalloligated clusters $[Pt_2M_2Cp_2(CO)_6(\eta^2\text{-dppe})]$ were obtained,[29a] whereas with $Ph_2PCH_2PPh_2$ (dppm) heterolytic cleavage of a Pt-M bond occurred, leading to the heterodinuclear complexes $[(\eta^2\text{-dppm})Pt(\mu\text{-dppm})M(CO)_2Cp]^+$ (M = Mo, W).[29b] These examples illustrate the versatility of these precursors and the geometrical control exerted by the phosphine ligand on the nuclearity and structure of the resulting mixed-metal complexes.

We have now found that the use of bulkier monodentate phosphine ligands (PCy_3, $P(i\text{-Pr})_3$, $P(m\text{-Tol})_3$, $P(CyPh_2)$, $P(p\text{-Tol})_3$ and $P(i\text{-Bu})_3$) still leads to clusters of the general formula $[Pt_2M_2Cp_2(CO)_6(PR_3)_2]$ but allows for the first time the observation of planar and tetrahedral isomers, which are interconvertible in solution. When the steric bulk of the phosphine is increased, folding of the metal core from planar to tetrahedral occurs, allowing a less congested situation.

That the isomers are interconvertible has been shown by ^{31}P NMR spectroscopic studies on solutions of clusters 1–5. Although the activation energies (ΔG^*) could not be determined for solubility

(27) (a) For a good introduction to this topic, see: Bueno, C.; Churchill, M. R. *Inorg. Chem.* **1981**, *20*, 2197 and references cited therein. (b) For $[\{CpMo(CO)_3\}_2Pb(THF)]$, see: Hitchcock, P. B.; Lappert, M. F.; Michalczyk, M. J. *J. Chem. Soc., Dalton Trans.* **1987**, 2635. (d) For $[\{CpMo(CO)_3\}_3In]$, see Clarkson, L. M.; Clegg, W.; Norman, N. C.; Tucker, A. J.; Webster, P. M. *Inorg. Chem.* **1988**, *27*, 2653. (e) For $[\{CpMo(CO)_3\}_2BiCl]$, see: Clegg, W.; Compton, N. A.; Errington, R. J.; Norman, N. C.; Tucker, A. J.; Winter, M. J. *J. Chem. Soc., Dalton Trans.* **1988**, 2941.

(28) Hirsi, D. M. In *Mathematics for Chemists*; The MacMillan Press LTD: London and Basingstoke, 1983.

(29) (a) Braunstein, P.; Jud, J.-M.; Dusausoy, Y.; Fischer, J. *Organometallics* **1983**, *2*, 180. (b) Braunstein, P.; de Méric de Bellefon, C.; Lanfranchi, M.; Tiripicchio, A. *Organometallics* **1984**, *3*, 1772.

reasons (see above), a lower value of ca. 18 kcal·mol^{-1} may be estimated from a coalescence temperature higher than 120 °C (e.g., no broadening was observed up to 110 °C for **4**) and a difference $|\nu_a - \nu_b|$ for the isomers a and b ranging from 227 Hz for **3** to 875 Hz for **1**.[30] Pertinent examples of interconvertible structures include clusters $[Fe_4(\mu\text{-A})(CO)_{13}]^-$ (A = HgMo(CO)$_3$Cp, HgCH$_3$) that display a related isomerization from butterfly to tetrahedron, although with change in the total electron count,[15] $[Os_4(\mu_3\text{-S})(CO)_{12}(HC_2Ph)]$, for which a similar activation energy has been found for its butterfly to rhombus chain isomerism ($\Delta G^{\ddagger}_{295}$ = 18.6 kcal·mol^{-1}),[11] and $[PtOs_3(\mu\text{-S})_2(CO)_9(PMe_2Ph)_2]$ ($\Delta G^{\ddagger}_{167}$ = 7.5 kcal·mol^{-1}),[32] $[Os_4(CO)_{14}(PMe_3)]$ ($\Delta G^{\ddagger}_{184}$ = 8.0 kcal·mol^{-1}),[33a] and $[PtOs_3(\mu\text{-H})_2(CO)_{11}(PCy_3)]$,[34] for which softer metal core deformations were found. The butterfly (Fe wingtip) to butterfly (Fe hinge) isomerization of $[FeRu_3N(CO)_{12}]^-$ ($\Delta G^{\ddagger}_{300}$ = 26.3 kcal·mol^{-1})[5d] was described as involving a square-pyramidal intermediate (analogous to the Berry pseudorotation) or a trigonal-bipyramidal intermediate, whereas the isomerization mechanism for clusters **1**–**5** relates more to the square–diamond–square (SDS) rearrangement, well-known in borane and carborane chemistry.[2,31] We shall return to this point later.

A particularly remarkable feature in the polytopal rearrangements described here is that the occurrence of stereoisomers, as well as their interconversion in solution, results only from steric factors, the electronic properties of the phosphines used being too similar to be invoked. This is interesting to contrast with previous examples where electronic factors only were invoked as (i) for the folding away from planarity in a series of Ru_4 butterfly clusters,[35] (ii) for the tetrahedron to butterfly isomerization in clusters $[Fe_4(\mu\text{-A})(CO)_{13}]^-$ (A = H, HgCH$_3$, AuPR$_3$, CuPR$_3$), where Shriver et al. found that the strongest electrophile produces the highest concentration of the butterfly isomer,[15] each isomer remaining electron precise as the TEC differs in the butterfly (62e) and the tetrahedron (60e), and (iii) for the preference of the puckered-square vs spiked-triangular metal framework in a series of clusters $[Os_4(CO)_{15}(L)]$ (L = CO, PF$_3$, P(OCH$_2$)$_3$CMe), dictated primarily by the electronic properties of L.[33b]

Electron Counting. The isomeric clusters presented here have a TEC of 58 of which 10e are involved in the bonding of the metallic core. Having two geometries with the same electron count is rather uncommon and raises the question of the change in the localization of bonding electrons within the metallic core when going from planar to tetrahedral geometries.

Thus, for the planar geometry, the EAN rule requires five 2e-2c metal–metal bonds in agreement with the X-ray data and the bonding description discussed previously.[24] Note that the planar isomer a nicely illustrates the cluster condensation rule, which stipulates that "the total electron count in a condensed polyhedron is equal to the sum of the characteristic electron counts for the parent polyhedra minus the electron count characteristic of the atom, pair of atoms, or face of atoms common to both polyhedra".[36] Isomer a can be viewed as the assembling of two triangles sharing a Pt–Pt edge (2 × 44 − 30 = 58).

For the tetrahedral geometry of isomer b, the EAN rule would require six 2e-2c metal–metal bonds and an electron count of 60 (4 × 18 − 6 × 2) or 56 (2 × 18(Mo) + 2 × 16(Pt) − 6 × 2). Within this rule, the observed electron count of 58 could only be rationalized (i) by considering an 18e and a 16e platinum center, thus invoking a dative Pt(18)→Pt(16) bond or (ii) by considering two 18e platinum centers and a double metal–metal bond in the framework. There is no structural argument from the X-ray data to support such views, thus making the EAN rule inoperant for isomers b.

These considerations lead to a first conclusion that the bonding in isomer a could be described as localized along the metal–metal edges with five 2e–2c bonds, making isomer a an "electron precise" cluster. The conclusion is different for isomer b, which displays a localization along the six edges with bond orders less than 1.

As pointed out by Fowler and Mingos, the tetrahedron has both of the deltahedral and the three-connected geometries.[37] Johnston and Mingos have shown that two electron counts are possible for this kind of C_3 polar N-vertex deltahedron: either N or $N + 2$ skeletal electron pairs, depending on the occupation or nonoccupation of a degenerate e level.[38] The large majority of tetrahedral clusters obey the $N + 2$ rule (i.e., TEC = 60) and are in fact "electron precise". However, a count of $N + 1$ skeletal electron pairs (TEC = 58) for the Pt_2Mo_2 clusters can be accommodated by assuming a partial occupation of the degenerate e set. This situation is obtained by a Jahn–Teller distortion of the ideal T_d symmetry, which can be realized by a flattening of the tetrahedron.[39] In fact, the X-ray data of **2b**, which shows four short (Mo–Pt) and two long (Mo–Mo and Pt–Pt) bonds is consistent with this view. Our MO calculations also support this idea (see below).

In the following, we shall try to examine the reasons for this unique behavior and see whether it could be related to a "buffer" ability of platinum to change its electron count from 16 to 18 between the two isomers. Due to the high-lying nature of the p orbitals of platinum, lower electron counts are found in platinum-containing clusters. Thus, the TEC should be 30 for a binuclear Pt_2, 42 or 44 in the triangular Pt_3, 56 in the tetrahedral Pt_4 system (the N skeletal pairs situation), etc., i.e., 4e less than in clusters made of transition metal obeying the 18e count.[40] However, it should be noted that tetrahedral Pt_4 clusters with less than 56e also exist.[41] The corresponding MO calculations also show that the ligand systems within the Pt_n clusters are of fundamental importance, π-donor bridging ligands (e.g., phosphido, halogeno, etc.) favoring higher electron counts by matching with the empty p acceptor orbitals of the platinum, contrary to π-acceptor bridging ligands like CO.[42]

Bonding Analysis. One of the cluster geometries encountered in this work, the planar triangulated rhombohedral (PTR) **2a**, is assigned on the basis of comparative solution NMR and crystallographic data. The other geometry is a distorted tetrahedron rather than a butterfly. Evidence comes from the crystal structure of **2b**, which depicts six metal–metal distances in the range usually found for the corresponding metal–metal bonds, and from the ^{31}P NMR data, which support a significant Pt–Pt interaction.[43] A similar distorted tetrahedral geometry is also adopted by some

(30) The $\Delta G^{\ddagger}$ value for the process observed via NMR spectroscopy was estimated by using the formula $\Delta G^{\ddagger} = (19 \times 10^{-3})Tc(9.97 + \log Tc - \log |\nu a - \nu b|)$ derived from the Eyring equation. See: Hesse, M.; Meier, H.; Zeeh, B. In *Spektroskopischen Methoden in der Organischen Chemie*; Georg Thieme Verlag Stuttgart: New York, 1984; p 133. Günther, H. In *NMR Spectroscopy!* Georg Thieme Verlag Stuttgart: New York, 1983; p 229.

(31) See, for example: (a) Gimarc, B. M.; Ott, J. J. *Inorg. Chem.* **1986**, *25*, 83. (b) Wales, D. J.; Stone, A. J. *Inorg. Chem.* **1987**, *26*, 3845. (c) Mingos, D. M. P.; Johnston, R. L. *Polyhedron* **1988**, *7*, 2437. (d) Wales, D. J.; Mingos, D. M. P.; Lin, Z. *Inorg. Chem.* **1989**, *28*, 2754.

(32) Adams, R. D.; Horváth, I. T.; Wang, S. *Inorg. CHem.* **1986**, *25*, 1617.

(33) (a) Martin, L. R.; Einstein, F. W. B.; Pomeroy, R. K. *Organometallics* **1988**, *7*, 294. (b) Einstein, F. W. B.; Johnston, V. J.; Pomeroy, R. K. *Ibid.* **1990**, *9*, 1754.

(34) Ewing, P.; Farrugia, L. J.; Rycroft, D. S. *Organometallics* **1988**, *7*, 859.

(35) Carty, A. J.; MacLaughlin, S. A.; van Wagner, J.; Taylor, N. J. *Organometallics* **1982**, *1*, 1013.

(36) Mingos, D. M. P.; Evans, D. G. *J. Organomet. Chem.* **1983**, *251*, C13.

(37) (a) Fowler, P. W.; Porterfield, W. W. *Inorg. CHem.* **1985**, *24*, 3511. (b) Johnston, R. L.; Mingos, D. M. P. *J. Organomet. Chem.* **1985**, *280*, 407.

(38) Johnston, R. L.; Mingos, D. M. P. *J. Chem. Soc., Dalton Trans.* **1987**, 1445.

(39) Cox, D. N.; Mingos, D. M. P.; Hoffmann, R. *J. Chem. Soc., Dalton Trans.* **1981**, 1788.

(40) Mingos, D. M. P.; Wardle, R. W. M. *Transition Met. Chem. (Weinheim, Ger.)* **1985**, *10*, 441 and references therein.

(41) (a) Mingos, D. M. P.; Evans, D. G. *J. Organomet. Chem.* **1982**, *240*, 321. (b) Mingos, D. M. P.; Johnston, R. L. *Struct. Bonding (Berlin)* **1987**, *68*, 30.

(42) Underwood, D. J.; Hoffmann, R.; Tatsumi, K.; Nakamura, A.; Yamamoto, Y. *J. Am. Chem. Soc.* **1985**, *107*, 5968.

(43) Although direct correlations between ^1J(PtPt) coupling and Pt–Pt distances are not possible,[44] the existence of a strong ^1J coupling implies a good overlap of the MO's centered on each platinum atom; for discussion, see: Pregosin, P. S. *Coord. Chem. Rev.* **1982**, *44*, 247 and references cited therein.

(44) (a) Boag, N. M.; Browning, J.; Crocker, C.; Goggin, P. L.; Goodfellow, R.; Murray, M.; Spencer, J. L. *J. Chem. Res., Miniprint* **1978**, 2962. (b) Moor, A.; Pregosin, P. S.; Venanzi, L. M. *Inorg. Chim. Acta* **1982**, *61*, 135.

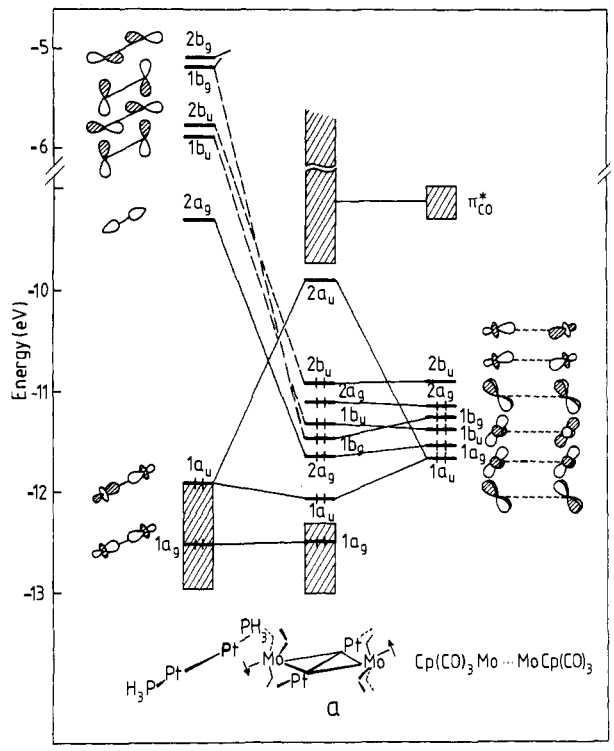

Figure 3. MO diagram of the planar, triangulated rhombohedral $Mo_2Pt_2Cp_2(CO)_6(PH_3)_2$ model, a (C_{2h} symmetry).

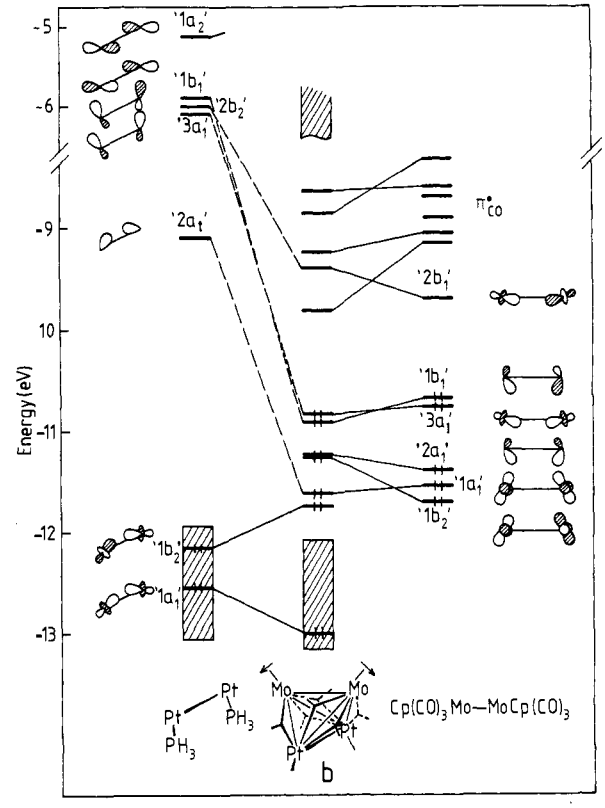

Figure 4. MO diagram of the tetrahedral $Mo_2Pt_2Cp_2(CO)_6(PH_3)_2$ model b. The symmetry is C_1. Fragment orbitals are labeled in the C_{2v} pseudosymmetry of the $Mo_2Pt_2Cp_2(PH_3)_2$ core.

other 58-electron mixed-metal clusters, such as $[Pt_2M_2(CO)_8(PR_3)_2(H)_n]$ (n = 2, M = Fe,[45a] Os;[45b] n = 0, Co[46]) and $[Pt_2Ir_2(CO)_7(PR_3)_3]$,[47] which also present ^{31}P NMR data similar to those of **1b–5b** (strong ^1J(PtPt) and very weak ^3J(PP)).

Extended Hückel molecular orbital calculations were carried out in order to better understand and compare the bonding features in both the a and b isomers of $[Pt_2M_2Cp_2(CO)_6(PH_3)_2]$. The computational details are given in the Experimental Section.

Planar Triangulated Rhombohedral Geometry. We first analyze the electronic structure of the model compound $[Pt_2Mo_2Cp_2(CO)_6(PH_3)_2]$ in the usually encountered planar triangulated rhombohedral geometry a (see Figure 3; the arrows represent the cyclopentadienyl ligands). This molecule can be constructed conceptually from the fragments $(CO)_3CpMo\cdots MoCp(CO)_3$ and $(H_3P)Pt–Pt(PH_3)$. The former fragment exhibits a set of six frontier molecular orbitals (FMO's), which are the in-phase and out-of-phase combinations of the "t_{2g}" set of the noninteracting $MoCp(CO)_3$ pseudooctahedral units[48] (see the right-hand side of Figure 3). Only the metal character of the FMO's has been represented for clarity, but they have also a rather important π^* carbonyl contribution, ca. 40–50%. The frontier orbitals of the Pt_2 fragment, represented on the left-hand side of Figure 3, result from the assembling of two mononuclear $PtPH_3$ units. ML fragments, such as $Pt(PH_3)$, possess a set of three diffuse s- and p-type orbitals ($\sigma + \pi$) lying high above the block of the 5d levels. Only the σ-type hybrids overlap strongly at a Pt–Pt separation of 2.65 Å. Their antibonding combination lies at very high energy and can be discarded; their bonding counterpart ($2a_g$) goes down enough to mix somewhat with the σ-bonding combination of the d levels. Thus, the Pt_2 entity presents five diffuse frontier orbitals above a nest of ten d levels. We would like to concentrate further on the Pt–Pt σ-type interactions: The metallic $1a_g$ d level has some s and p character mixed in and therefore is rather bonding (Pt–Pt overlap population (OP) 0.116). This is not the case of the $1a_u$ MO, which is weakly antibonding (OP −0.043). Finally, the hybrid $2a_g$ level is strongly bonding (OP 0.616).

The interaction of the two dinuclear moieties leads to a stable model for the expected 58-electron count. A HOMO–LUMO gap of 0.9 eV is computed. Significant stabilizing interactions occur between the five diffuse Pt_2 frontier orbitals and five orbitals among the six Mo_2 FMO's, but the major interaction involves the two $1a_u$ levels. This strong interaction results from a close energy matching rather than from the overlap, which is very poor (0.02). Consequently, the out-of-phase combination is vacant and constitutes the LUMO of the complex. This leads to a significant depopulation of the σ^*-antibonding $1a_u$ level of the Pt_2 entity (occupation of 1.08e after interaction). The depopulation of the Pt_2 $1a_u$ FMO together with the population of the Pt_2 $2a_g$ FMO (0.55e in the complex) contributes to the formation of a strong Pt–Pt σ bond. A total Pt–Pt overlap population of 0.200 is computed in isomer a. This is consistent with the short Pt–Pt distances observed in this series of compounds.[24b,49] Another consequence of the vacancy of $2a_u$ in isomer a is the occupation of the $2b_u$ FMO of the Mo_2 moiety, which was empty before interaction. Its occupation corresponds to an electron donation from platinum to molybdenum atoms. Additional electron transfer from the Pt_2 entity toward the Mo_2 unit occurs from the interaction of occupied Pt d MO's with the vacant π^* orbitals of the semibridging carbonyl ligands. Indeed the computed overlap populations between the platinum and the carbon atoms of the carbonyls indicate that important "through-bridge" bonding must be present in isomer a. The average Pt···C(O) overlap population is 0.21.

An effective electron transfer of 2.26e occurs from the d block of the Pt_2 entity toward the Mo_2 moiety, while the Pt_2 s- and p-type

(45) (a) Farrugia, L. J.; Howard, J. A. K.; Mitrprachachon, P.; Stone, F. G. A.; Woodward, P. *J. Chem. Soc., Dalton Trans.* **1981**, 1134. (b) Farrugia, L. J.; Howard, J. A. K.; Mitprachachon, P.; Stone, F. G. A.; Woodward, P. *J. Chem. Soc., Dalton Trans.* **1981**, 1274.

(46) (a) Fischer, J.; Mitschler, A.; Weiss, R.; Dehand, J.; Nennig, J.-F. *J. Organomet. Chem.* **1975**, *91*, C37. (b) Braunstein, P.; Dehand, J.; Nennig, J. F. *J. Organomet. Chem.* **1975**, *92*, 117.

(47) Bhadurl, S.; Sharma, K. R.; Clegg, W.; Sheldrick, G. M.; Stalke, D. *J. Chem. Soc., Dalton Trans.* **1984**, 2851.

(48) Hofmann, P.; Schmidt, H. R. *Angew. Chem., Int. Ed. Engl.* **1986**, *25*, 837.

(49) Bouaoud, S.-E. Thèse d'Etat. Rennes, 1987.

FMO's accept 1.12e from the Mo_2 fragment. The net electron donation of more than 1 electron from the Pt_2 system toward the Mo_2 unit is in agreement with infrared data on this type of clusters, showing that the $MoCp(CO)_3$ fragments are very electron rich.[24]

Occupied MO's in the HOMO region are mainly localized on the two Mo atoms and thus are mainly nonbonding. On the other hand, the $2a_u$ LUMO, possessing an important contribution on both Pt and Mo atoms, is strongly antibonding. This corroborates the electrochemical studies carried out on this type of clusters. The reduction of the PTR $[Pt_2M_2Cp_2(CO)_6(PR_3)_2]$ compounds is followed by immediate chemical decomposition, while oxidized Pt_2M_2 cluster species have been identified.[50]

Tetrahedral Geometry. The interaction diagram corresponding to the tetrahedral structure b is shown in Figure 4. Before entering into its analysis, it is important to note that the symmetry group of structure b is C_1 because of the very unsymmetrical arrangement of the carbonyl ligands. However, a rough C_{2v} pseudosymmetry can be considered if one neglects the CO ligands.

The energies and space localizations of the Pt_2 FMO's in isomer b are not very different from the PTR case. The small differences observed are caused by the bending of the P–Pt–Pt angle, which is now 140°. The FMO's of the Mo_2 fragment are more perturbed when going from structure a to b. The close Mo–Mo contact (3.13 Å) splits the σ/σ^* levels. Moreover, the different arrangements of the carbonyl ligands modify the orientation and the composition of the "t_{2g}" orbitals.

The five low-lying FMO's of the Mo_2 unit are somewhat stabilized by the five high-lying Pt_2 levels, while in contrast to the PTR case the high-lying Mo–Mo σ^* "$2b_1$" orbital correlates with a vacant MO in the complex. Consequently the total overlap population between the two molybdenum atoms is rather important (0.12) and compares favorably with that found in the dimer $[Mo(CO)_3Cp]_2$ (0.11, for an Mo–Mo separation of 3.13 Å in both cases). This supports the view of a significant Mo–Mo interaction in isomer b. The other major difference with the PTR structure is the absence of any strong interaction involving the Pt–Pt σ^* "b_2" frontier orbital. The overlap between the two "$1b_2$" FMO's is almost zero, and consequently no significant splitting occurs between these levels, which are found both occupied in the complex. Similarly to structure a, a HOMO–LUMO gap of 1.0 eV is observed for isomer b. The HOMO is mainly localized on the two Mo centers. The LUMO is mainly made of ligand contributions.

To summarize, in structure b, the Mo–Mo σ^* orbital is vacant and the Pt–Pt σ^* one is occupied, while in structure a the Mo–Mo σ^* is occupied and the LUMO has a strong Pt–Pt σ^*-antibonding character. Clearly, some kind of level crossing occurs when going from isomer a to b, which is to some extent related to the square–diamond–square transformation.[2,31]

The question that arises then is why is there still some Pt···Pt bonding in isomer b. The answer lies in the weak antibonding character of the Pt–Pt σ^* "$1b_2$" FMO. Its population of 1.83e in the complex is not sufficient by itself to break the bond fully. Remember also that its dissociative effect is balanced by the participation of the Pt–Pt σ-bonding "$2a_1$" FMO into occupied levels (its population is 0.42e in the complex). Nonetheless, this leads to an important weakening in the Pt–Pt bonding. The overlap population between the two platinum atoms decreases from 0.20e in structure a to 0.14 e in structure b (when keeping the same Pt–Pt distance of 2.65 Å in both calculations). The weakening of the Pt–Pt overlap population is in agreement with the observed lengthening of the Pt–Pt vector in the tetrahedral cluster, 2.99 Å against ca. 2.65 Å in the PTR clusters. It is interesting to note that a complete breaking of the Pt–Pt bond, i.e., a butterfly or a PTR structure with an Mo–Mo hinge, will not change fundamentally the electronic structure of isomer b. The partial Pt–Pt bonding observed in the title compound might result from a compromise between various electronic and steric factors. An analogous situation is encountered in the 58e compounds $[Pt_2M_2(CO)_8(PR_3)_2(H)_2]$ (M = Fe, Os),[45] $[Pt_2Co_2(CO)_8(PPh_3)_2]$,[46] and $[Pt_2Ir_2(CO)_7(PPh_3)_3]$.[47] Because of the range of the Pt–Pt separations from 2.97 to 3.21 Å, these clusters are generally viewed as having a butterfly rather than a tetrahedral structure, with M atoms occupying the hinge and Pt atoms the wingtip positions. So, the title compound belongs also to this class of clusters, where a 58e count can be observed over a large range of Pt–Pt distances, i.e., for both tetrahedral and butterfly structures.

Finally, it should be noted that, as in isomer a, a net electron transfer of more than 1e occurs in structure b, from the Pt_2 unit toward the Mo_2 entity. Here again, the π^* levels of the semibridging carbonyl ligands are involved in the transfer.

Discussion of the Structure–Bonding Relationship. Both planar triangulated rhombohedral and tetrahedral structures favor a 58e count. Our calculations find the PTR model preferred by about 1 eV. However, the preference of one particular geometry must depend critically upon the geometrical factors imposed by the tertiary phosphines coordinated to the Pt atoms. Bulky tricyclohexylphosphine ligands probably induce a lengthening of the Pt–Pt distance in order to avoid steric hindrance with the $MoCp(CO)_3$ fragments. The result is a loss in the platinum–platinum bonding, which must be compensated by partial formation of a molybdenum–molybdenum bond. The example of the more open, metalloligated triangular structure of $[Pt_2Mo_2Cp_2(CO)_6(\eta^2\text{-dppe})]$, also possessing 58e, illustrates the important role exerted by the nature of the phosphine ligands on the structure of the mixed-metal Pt_2M_2 compounds.[29a]

As explained above, the a $\rightleftarrows$ b interconversion is accompanied by a level crossing between occupied and vacant MO's. However, since no symmetry element is present in isomer b, the crossing is avoided. This should give rise to an energy barrier consistent with the two forms a and b being true isomers able to coexist in equilibrium in solution. The experimental observation that this interconversion is rapid suggests that the height of this barrier is moderate, in agreement with the expected very low symmetry of the transition state.

Finally, the bonding mode in these compounds deserves further comment related to the electron-counting procedures. A localized bonding scheme for the 58e PTR compound a would require five metal–metal bonds corresponding to five metal cluster orbitals, two a_g, one a_u, one b_g, and one b_u. Thus, we are tempted to find five MO's in the diagram of form a that are principally responsible for the formation of the metal–metal bonds. Analysis of the MO diagram of compound a (Figure 3) reveals firstly that the lowest MO ($1a_g$) corresponds to the Pt–Pt bond. Then the four following MO's (going up in energy; $1a_u$, $2a_g$, $1b_g$, and $1b_u$), which result from the interaction of four Mo_2 FMO's with symmetry-related Pt_2 levels with a major Mo_2 contribution, can be assigned to the four Mo–Pt contacts. The two remaining occupied MO's ($2a_g$ and $2b_u$) are almost purely the Mo···Mo σ and σ^* combinations and can be considered as nonbonding orbitals. This supports the view that the two $[Mo(CO)_3Cp]^-$ groups behave as 4e donor entities bridging the $[Pt_2(PR_3)_2]^{2+}$ moiety. Such a bonding mode has been proposed for the series of clusters $[Pt_2M_2Cp_2(CO)_6(PR_3)_2]$ (M = Cr, Mo, W; R = Me, Et, *n*-Bu, Ph)[24b] and is similar to that found for other anionic 4e donor bridging ligands like η^3-cyclopentadienyl,[51] phosphido,[52] and π-allyl (Scheme IIa).[53]

The situation in the 58e tetrahedral compound b is rather different. We still have only 10 "bonding" electrons, and a localized bonding scheme would lead to two extreme cases, one with a Mo–Mo bond and no Pt–Pt contact and the other with a Pt–Pt bond but no Mo–Mo bond. In the first case, the Mo_2 unit would give 8e to the Pt_2 moiety, in the latter only 6e (Scheme

(50) Jund, R.; Lemoine, P.; Gross, M.; Bender, R.; Braunstein, P. *J. Chem. Soc., Dalton Trans.* **1985**, 711.

(51) (a) For the X-ray characterization, see: Werner, H.; Kraus, H.-J. *J. Chem. Soc., Chem. Commun.* **1979**, 814. (b) For a review on Cp and π-allyl ligands coordinated to $[M(PR_3)]_2$ (M = Pd, Pt), see: Werner, H. *Adv. Organomet. Chem.* **1981**, *19*, 155.

(52) Taylor, N. J.; Chieh, P. C.; Carty, A. J. *J. Chem. Soc., Chem. Commun.* **1975**, 448.

(53) Jolly, P. W.; Krüger, C.; Schick, K.-P.; Wilke, G. *Z. Naturforsch.* **1980**, *35B*, 926.

Scheme II

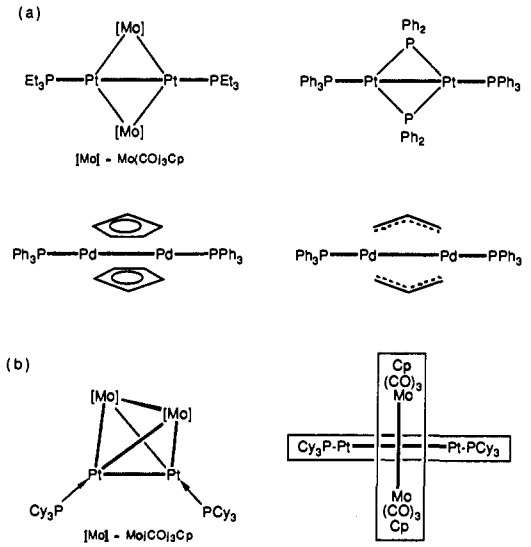

IIb). The true situation is somewhere in between since formally some partial Pt–Pt and Mo–Mo bonding is observed and calculated to exist in the isomer b. Therefore, four MO's among the six highest occupied MO's shown in Figure 4 must correspond to the four Mo–Pt bonds of isomer b, while the lowest MO positioned in the d block deriving principally from the "$1a_1$ FMO of the Pt_2 unit could be considered as having the 2 delocalized electrons participating to the partial Mo–Mo and Pt–Pt bonds.

Considering the platinum atoms as 18e centers (see the Electron Counting subsection) implies that the high-lying p orbitals of the platinum atoms participate in the bonding. This second approach is supported by our molecular orbital calculations, which have revealed a strongly bonding interaction between the "p-like" orbitals of the $Pt_2(PH_3)_2$ fragment and the π-donor orbitals of the $[Cp(CO)_3Mo]\cdots[Mo(CO)_3Cp]$ fragment, making it a π donor in both isomers a and b. However, from the MO diagram of isomer a shown in Figure 3, one may notice that the empty $2b_u$ FMO of the Mo···Mo fragment accepts formally 2 electrons from the $1a_u$ FMO of the Pt–Pt unit to afford the $2b_u$ MO of isomer a. Note that this "π-like acceptor" character of the $[MoCp(CO)_3]_2$ entity is somewhat reduced by electron transfer to the p orbital of the Pt_2 unit. The situation is rather different in isomer b, where the Mo_2 π-like $1b_1$ and $3a_1$ FMO's are electron donor toward the empty p-like $3a_1$ and $1b_1$ MO's of the Pt–Pt unit (see above for more details). Thus, the two $[Mo(CO)_3Cp]$ metalloligands in isomer a are more "π-acceptor-like" favoring a lower electron count (58e, instead of 60e, electron precise with two 16e Pt centers), whereas the $[Mo(CO)_3Cp]_2$ metalloligand in structure b is more "π-donor-like" favoring a higher electron count (58e, instead of 56e, requires 2 × 16e Pt centers and 2 × 18e Mo centers). This can be interpreted by the fact that the Pt_2 σ^* frontier orbital is vacant in isomer a but occupied in b. We may also view the structural change as resulting from an intramolecular reaction induced by the steric properties of the $(PR_3)Pt$–$Pt(PR_3)$ fragment that would convert two mononuclear $Mo(CO)_3Cp$ metalloligands into a dinuclear $[Mo(CO)_3Cp]_2$ metalloligand. The latter fragment, having less π-acceptor capacity than the former, is now able to stabilize a tetrahedral geometry with the same 58e count. This should be compared with the intramolecular change of CO coordination from η^1 to η^1-μ_2, accompanied by a change in the electron count from 60 to 62e, respectively, that occurred during the butterfly to tetrahedral core isomerization of the $[Fe_4(\mu\text{-}A)(CO)_{13}]^-$ clusters.[15] Finally, it should be pointed out that the structures of isomers a and b, having the same electron count, represent "snapshots" of intermediates (or transition states) involved in cluster dynamics.[54]

(54) See, for example: Moor, A.; Pregosin, P. S.; Venanzi, L. M.; Welch, A. J. *Inorg. Chim. Acta* **1984**, *85*, 103.

Experimental Section

All reactions were performed in Schlenk-type flasks under oxygen- and water-free nitrogen. Solvents were dried and distilled under nitrogen: tetrahydrofuran and diethyl ether over sodium benzophenone ketyl, *n*-hexane and pentane over sodium, dichloromethane and chloroform over P_2O_5. Infrared spectra were recorded on a Perkin-Elmer 398 spectrophotometer as KBr pellets or THF solutions. The ^1H, $^{31}P\{^1H\}$, and $^{195}Pt\{^1H\}$ NMR spectra were recorded at 200.13, 81.02, and 42.95 MHz, respectively, on a FT-Bruker WP SY200 instrument and externally referenced to Me_4Si, 85% H_3PO_4 in D_2O, and 0.3 M K_2PtCl_4 in D_2O, respectively, with downfield chemical shifts reported as positive. All NMR solvents were freeze–pump–thaw degassed before recording spectra. The complexes $Na[Mo(CO)_3(\eta\text{-}C_5H_4CH_3)]\cdot 2DME$ and *trans*-$[Pt\{Mo(CO)_3((\eta\text{-}C_5H_4CH_3)\}_2(PhCN)_2]$ were prepared as previously described for the analogous complexes $Na[M(CO)_3(\eta\text{-}C_5H_5)]$ and *trans*-$[Pt\{M(CO)_3(\eta\text{-}C_5H_5)\}_2(PhCN)_2]$ (M = Mo, W).[24] The phosphine ligands (Strem Chemicals) were used as received. Column chromatography was performed under nitrogen by using silica gel as support (Kieselgel 60, Merck). Elemental analyses were performed by the Service Central de Microanalyse du CNRS.

$[Pt_2Mo_2(\eta\text{-}C_5H_5)_2(CO)_6(PCy_3)_2]$ (1). A solution of PCy_3 (0.640 g, 2.28 mmol) in THF (10 mL)) was added to a suspension of *trans*-$[Pt\{Mo(CO)_3Cp\}_2(PhCN)_2]$ (1.89 g, 2.12 mmol) in THF (50 mL). The solution was stirred under reflux for 3 h. The solvent was removed in vacuo. The resulting red residue was chromatographed. Elution was performed with use of mixtures of CH_2Cl_2 and *n*-hexane, whose respective proportions are given in parentheses. The first elution (1:10) produced a red solution of $[Mo(CO)_3(\eta\text{-}C_5H_5)]_2$ (0.350 g, 0.720 mmol, 34% yield based on Mo). The second elution (2:10) afforded the orange-red cluster $[Pt_3(CO)_3(PCy_3)_3]$ (0.045 g, 0.030 mmol, 4% yield based on Pt). The main fraction (1:1) gave the red cluster **1** (0.730 g, 0.506 mmol, 48% based on Pt, 24% based on Mo): IR (KBr) ν(CO) 1802 (vs), 1731 (vs); (THF) 1797 (vs), 1731 (vs) cm^{-1}; ^1H NMR ($CDCl_3$) (**1a** was not observed) **1b** δ 5.24 (s, 10 H, C_5H_5, J(PtH) = 3.5 Hz), 2.30, 1.64 and 1.00 (m, 66 H, PC_6H_{11}); $^{195}Pt\{^1H\}$ NMR ($CDCl_3$) **1a** was not observed; **1b** δ 2483 (^1J(PtPt) = 1998 Hz). Anal. Calcd for **1**·0.5 CH_2Cl_2, $C_{52.5}H_{77}ClMo_2O_6P_2Pt_2$ (M_r = 1441.17): C, 42.50; H, 5.23; Mo, 12.93; P, 4.17; Pt, 26.29. Found: C, 41.71; H, 5.15; Mo, 12.57; P, 4.06; Pt, 25.56. Further elution with THF produced, after evaporation of the solvent, a brown powder (0.230 g, 9% of the total mass of the starting materials). The $^{31}P\{^1H\}$ NMR spectrum of this powder in $CDCl_3$ revealed the presence of the bimetallic complex $[PtCl\{Mo(CO)_3Cp\}(CO)(PCy_3)]$ (estimated yield 5% based on Pt) and of unidentified compounds.

$[Pt_2Mo_2(\eta\text{-}C_5H_4CH_3)_2(CO)_6(PCy_3)_2]$ (2). A solution of PCy_3 (0.32 g, 1.15 mmol) in THF (20 mL) was added to a suspension of *trans*-$[Pt\{Mo(CO)_3(\eta\text{-}C_5H_4CH_3)\}_2(PhCN)_2]$ (1.00 g, 1.09 mmol) in THF (50 mL). After being refluxed for 3 h, the red-orange solution was evaporated to dryness in vacuo. The red residue was chromatographed with use of the same procedure as for **1**. The first elution (1:10) produced a red solution of $[Mo(CO)_3(\eta\text{-}C_5H_4CH_3)]_2$ (0.120 g, 0.40 mmol, 37% yield based on Mo). As before, the second elution (2:10) afforded $[Pt_3(CO)_3(PCy_3)_3]$. The third elution (1:1) gave a red-orange solution, which was shown by $^{31}P\{^1H\}$ NMR to be a 10:1 mixture of **2** and of the bimetallic complex $[PtCl\{Mo(CO)_3Cp'\}(CO)(PCy_3)]$, respectively. Fortunately, these compounds present different solubilities, and cluster **2** could be precipitated from a mixture of CH_2Cl_2 and *n*-hexane at room temperature after a few days, while the bimetallic complex crystallized at −20 °C. Data for **2**: yield 0.30 g, 0.20 mmol, 38% based on Pt; mp 143 °C; IR (KBr) ν(CO) 1790 (br s), 1728 (s); (THF) 1789 (vs), 1729 (vs) cm^{-1}; ^1H NMR ($CDCl_3$) (**2a** was not observed) δ 5.04 (m, 4 H, C_5H_4), 2.07 (s, 6 H, CH_3), 2.26, 1.56 and 1.12 (m, 66 H, PC_6H_{11}). Anal. Calcd for $C_{54}H_{80}Mo_2O_6P_2Pt_2$ (M_r = 1469.25): C, 44.15; H, 5.49. Found: C, 44.54; H, 5.82.

$[Pt_2W_2(\eta\text{-}C_5H_5)_2(CO)_6(PCy_3)_2]$ (3). A reddish mixture of *trans*-$[Pt\{W(CO)_3Cp\}_2(PhCN)_2]$ (1.31 g, 1.23 mmol) and PCy_3 (0.38 g, 1.35 mmol) in THF (50 mL) was refluxed for 3 h. The solvent was removed under vacuum, and the red-brown residue was adsorbed onto silica by using CH_2Cl_2 (20 mL)/silica gel (20 mL). The solvent was removed in vacuo, and the solid was chromatographed on a 32 × 2.5 cm silica gel column. Elution was carried out with mixtures of CH_2Cl_2 and *n*-hexane, whose proportions are given in parentheses. The first fraction (1:2) contained the red-violet dimer $[W(CO)_3Cp]_2$ (0.30 g, 0.44 mmol, 36% yield based on W). Elution with a (2:1) mixture produced first the second fraction (orange solid, 0.05 g), which was not further investigated, and the third fraction from which the red-brown cluster **3** was isolated as a microcrystalline powder (0.52 g, 0.32 mmol, 52% yield based on Pt): IR (KBr) ν(CO) 1804 (vs), 1728 (vs) cm^{-1}; ^1H NMR ($CDCl_3$) (**3a** and **3b** are not differenciated) δ 5.30 (s, 10 H, C_5H_5), 2.26 and 1.89–1.12 (m, 66 H, PC_6H_{11}). Anal. Calcd for $C_{52}H_{76}O_6Pt_2W_2$ (M_r = 1616.98): C, 38.63; H, 4.74. Found: C, 38.15; H, 4.75. Elution with THF afforded

a dark brown mixture (0.18 g, 10% of the weight of the starting materials) containing [PtCl{W(CO)$_3$Cp}(CO)(PCy$_3$)] (IR evidence, IR (THF) ν(CO) 2047 (m), 1956 (s), 1879 (s) cm^{-1}).

[Pt$_2$Mo$_2$Cp$_2$(CO)$_6$[P(*i*-Pr)$_3$]$_2$] (4). A reddish mixture of *trans*-[Pt{Mo(CO)$_3$Cp}$_2$(PhCN)$_2$] (1.630 g, 1.81 mmol) and P(*i*-Pr)$_3$ (0.644 g, 4.02 mmol) in THF (50 mL) was refluxed for 4 h. After removal of the solvent in vacuo, the red-brown residue was chromatographed on a silica gel column (Kieselgel 60; 0.063–0.200 mm) with use of mixtures of CH_2Cl_2 and *n*-hexane. The first elution (1:9) gave [Mo(CO)$_3$Cp]$_2$ (0.300 g, 0.31 mol, 34% based on Mo). The second elution (1:1) afforded a light yellow solution, which was not further investigated. The main fraction was obtained by elution with a 9:1 mixture, and pure CH_2Cl_2 and was shown (by ^{31}P NMR) to contain the tetranuclear cluster [Pt$_2$Mo$_2$Cp$_2$(CO)$_6$[P(*i*-Pr$_3$)$_2$]] (**4**). Recrystallization from toluene (20 mL) at −25 °C afforded a brown microcrystalline powder of **4** (0.410 g, 0.34 mmol, 38% based on Pt). IR (KBr) ν(CO) 1892 (w), 1797 (s), 1729 (s) cm^{-1}; ^{1}H NMR ($CDCl_3$) (**4a**:**4b** = 2:3), **4a** δ 5.23 (s, 10 H, C_5H_5), 2.54 (m, 6 H, CH), 1.20 (dd, 36 H, CH_3, J(HH) = 7.2 Hz, J(PH) = 13.8 Hz); **4b** δ 5.25 (s, 10 H, C_5H_5, J(PtH) = 3.6 Hz), 2.54 (m, 6 H, CH), 0.95 (dd, 36 H, CH_3, J(HH) = 7.2 Hz, J(PH) = 14.4 Hz). Anal. Calcd for $C_{34}H_{52}Mo_2O_6P_2Pt_2$ (M_r = 1200.77): C, 34.01; H, 4.36. Found: C, 34.25; H, 4.32.

[Pt$_2$W$_2$Cp$_2$(CO)$_6$[P(*i*-Pr)$_3$]$_2$] (5). A solution of P(*i*-Pr)$_3$ (0.330 g, 2.06 mmol) in THF (10 mL) was added to a suspension of *trans*-[Pt{W(CO)$_3$Cp}$_2$(PhCN)$_2$] (1.98 g, 1.86 mmol) in THF (100 mL). The reddish mixture was refluxed for 3 h after which time the THF was removed in vacuo. The red-brown residue was chromatographed on a silica gel column (55 × 300 mm). Elution with a mixture of CH_2Cl_2 and *n*-hexane (1:2) afforded [W(CO)$_3$Cp]$_2$ (0.54 g, 0.80 mmol, 43% yield based on W). Following this fraction, a light yellow band was observed but not further investigated. Elution with a mixture of CH_2Cl_2 and *n*-hexane (3:1) afforded an orange solid (0.300 g), which contained a mixture of the dimer [W(CO)$_3$Cp]$_2$ and the cluster [Pt33(CO)$_3$(P(*i*-Pr)$_3$)$_3$]. Elution with a mixture of CH_2Cl_2 and THF (100:1 v/v) produced a large brown band from which a microcrystalline powder of cluster **5** was obtained after recrystallization in toluene (10 mL) (0.270 g, 0.20 mmol, 21% based on Pt). Elution with THF afforded a brown mixture that contained [PtCl$_2$(P(*i*-Pr)$_3$)$_2$] and [PtCl{W(CO)$_3$Cp}(CO)(P(*i*-Pr)$_3$)] (IR and ^{31}P NMR evidence). Data for **5**: IR (KBr) ν(CO) 1885 (m), 1847 (m), 1783 (s), 1749 (m), 1729 (s) cm^{-1}. ^{1}H NMR ($CDCl_3$) (**5a**:**5b** = 2:1) **5a** δ 5.32 (s, 10 H, C_5H_5), 2.44 (m, 6 H, CH), 1.20 (dd, 36 H, CH_3, J(HH) = 7.2 Hz, J(PH) = 13.8 Hz); **5b** δ 5.32 (s, 10 H, C_5H_5), 2.61 (m, 6 H, CH), 0.98 (dd, 36 H, CH_3, J(HH) = 7.2 Hz, J(PH) = 14.2 Hz). Anal. Calcd for $C_{34}H_{52}O_6P_2Pt_2W_2$ (M_r = 1376.59): C, 29.67; H, 3.81. Found: C, 30.04; H, 3.83.

[Pt$_2$Mo$_2$Cp$_2$(CO)$_6$(PCyPh$_2$)$_2$] (6). A reddish mixture of *trans*-[Pt{Mo(CO)$_3$Cp}$_2$(PhCN)$_2$] (1.67 g, 1.87 mmol) and PCyPh$_2$ (0.542 g, 1.97 mmol, 5% excess) in THF (100 mL) was refluxed for 4 h after which time the solvent was removed in vacuo. The dark residue was washed three times with a mixture of CH_2Cl_2 (15 mL) and *n*-hexane (40 mL) and twice with toluene (40 mL) to give a green solid. It was recrystallized from a mixture of CH_2Cl_2 (30 mL) and *n*-hexane (70 mL) to afford dark crystals of **6** (0.740 g, 0.52 mmol, 56% based on Pt): IR (KBr) ν(CO) 1888 (w), 1816 (br s), 1733 (s) cm^{-1}; ^{1}H NMR ($CDCl_3$) δ 7.52 to 7.36 (br m, 20 H, C_6H_5), 4.80 (s, 10 H, C_5H_5), 2.75, 1.96, 1.67, 1.33 and 0.93 (m, 22 H, PC_6H_{11}). Anal. Calcd for $C_{52}H_{52}Mo_2O_6P_2Pt_2$ (M_r = 1416.97): C, 44.08; H, 3.70. Found: C, 44.16; H, 3.73.

[Pt$_2$Mo$_2$Cp$_2$(CO)$_6$[P(*m*-Tol)$_3$]$_2$] (7). A reddish mixture of *trans*-[Pt{Mo(CO)$_3$Cp}$_2$(PhCN)$_2$] (0.896 g, 1.00 mmol) and P(*m*-Tol)$_3$ (0.336 g, 1.10 mmol) in THF (70 mL) was refluxed for 3 h. After the mixture was cooled and the solvent partially removed in vacuo, a green powder of **7** formed which was collected by filtration (0.481 g, 0.32 mmol, 64% based on Pt): IR (KBr) ν(CO) 1823 (br s), 1761 (s) cm^{-1}; ^{1}H NMR ($CDCl_3$) δ 7.50–7.20 (m, 24 H, C_6H_4), 4.64 (s, 10 H, C_5H_5), 2.31 (s, 18 H, CH_3). Anal. Calcd for $C_{58}H_{52}Mo_2O_6P_2Pt_2$ (M_r = 1489.07): C, 46.78; H, 3.52. Found: C, 47.28; H, 3.57.

[Pt$_2$Mo$_2$Cp$_2$(CO)$_6$[P(*p*-Tol)$_3$]$_2$] (8). A reddish mixture of *trans*-[Pt{Mo(CO)$_3$Cp}$_2$(PhCN)$_2$] (1.06 g, 1.19 mmol) and P(*p*-Tol)$_3$ (0.40 g, 1.31 mmol) in THF (70 mL) was refluxed for 3.5 h. After the mixture was cooled and stirred overnight at room temperature, a green microcrystalline powder of **8** formed and was collected by filtration (0.61 g, 0.41 mmol, 69% based on Pt): IR (KBr) ν(CO) 1825 (vs, br), 1747 (s) cm^{-1}; ^{1}H NMR ($CDCl_3$) δ 7.40 (m) and 7.14 (d, 24 H, C_6H_4), 4.65 (s, 10 H, C_5H_5), 2.35 (s, 18 H, CH_3). Anal. Calcd for $C_{58}H_{52}Mo_2O_6P_2Pt_2$ (M_r = 1489.07): C, 46.78; H, 3.52. Found: C, 46.93; H, 3.54.

[Pt$_2$Mo$_2$Cp$_2$(CO)$_6$[P(*i*-Bu)$_3$]$_2$] (9). P(*i*-Bu)$_3$ (0.36 g, 1.78 mmol) was added via syringe to a suspension of *trans*-[Pt{Mo(CO)$_3$Cp}$_2$(PhCN)$_2$] (1.18 g, 1.32 mmol) in THF (100 mL). The mixture was refluxed for 2 h after which time the solvent was removed in vacuo. The red-brown residue was extracted three times with a mixture of CH_2Cl_2 (20 mL) and *n*-hexane (20 mL), leaving poorly soluble crystals of [Mo(CO)$_3$Cp]$_2$ (0.19 g, 0.39 mmol, 30% based on Mo). The concentrated filtrate was chromatographed on a 30 × 2 cm silica gel column and eluted with a 1:1 mixture of CH_2Cl_2 and *n*-hexane. Only one fraction was collected and shown to contain cluster **9** and a trace amount of [Mo(CO)$_3$Cp]$_2$. This was washed with Et_2O and recrystallized from toluene (20 mL), yielding a red-brown microcrystalline powder of **9** (0.22 g, 0.17 mmol, 26% based on Pt): IR (KBr) ν(CO) 1812 (br s), 1718 (s) cm^{-1}; ^{1}H NMR ($CDCl_3$) δ 5.18 (s, 10 H, C_5H_5), 1.85 (m, 18 H, CH_2CH), 0.94 (d, 36 H, CH_3, J(HH) = 6.3 Hz). Anal. Calcd for $C_{40}H_{64}Mo_2O_6P_2Pt_2$ (M_r = 1284.93): C, 37.39; H, 5.02. Found: C, 37.28; H, 4.88.

Attempted Reaction of *trans*-[Pt{Mo(CO)$_3$Cp}$_2$(PhCN)$_2$] with P(*o*-Tol)$_3$. A reddish mixture of *trans*-[Pt{Mo(CO)$_3$Cp}$_2$(PhCN)$_2$] (0.303 g, 0.340 mmol) and P(*o*-Tol)$_3$ (0.118 g, 0.388 mmol) in THF (40 mL) was refluxed for 3.5 h. The solvent was removed in vacuo, and a ^{31}P{^{1}H} NMR spectrum (CD_2Cl_2) of the mixture only showed the presence of free phosphine (δ = −29.1 ppm). Overnight refluxing in toluene only resulted in decomposition to Pt(0) (metallic mirror) and [Mo(CO)$_3$Cp]$_2$.

Computational Procedures. The calculations were carried out within the extended Hückel formalism[55] with use of the weighted H_{ij} formula.[56]

Table V. Extended Hückel Parameters

orbital		H_{ii} (eV)	exponents[a] ζ_1	ζ_2
H	1s	−13.60	1.30	
C	2s	−21.40	1.625	
	2p	−11.40	1.625	
O	2s	−32.30	2.275	
	2p	−14.80	2.275	
P	3s	−18.60	1.60	
	3p	−14.00	1.60	
Mo	5s	−8.34	1.96	
	5p	−5.24	1.92	
	4d	−10.50	4.54 (0.5900)	1.90 (0.5900)
Pt	6s	−9.077	2.554	
	6p	−5.475	2.535	
	5d	−12.59	6.013 (0.6334)	2.696 (0.5513)

[a] Coefficients of double-ζ expansion in parentheses.

Table VI. Crystal Data and Intensity Collection Parameters for **2b**

compd	[Pt$_2$Mo$_2$Cp'$_2$(CO)$_6$(PCy$_3$)$_2$] (**2b**)
formula	$C_{54}H_{80}Mo_2O_6P_2Pt_2$
fw	1469.25
cryst syst	monoclinic
space group	$P2_1/n$
cyrst dimens, mm	0.40 × 0.15 × 0.15
a, (Å)	10.321 (3)
b, (Å)	24.351 (8)
c, (Å)	21.368 (6)
β, deg	92.76 (4)
V, (Å^3)	5364
Z	4
F(000) (e)	2888
ρ(calcd.) (g·cm^{-3})	1.819
temp (°C)	25
diffractometer	Enraf-Nonius CAD-4
radiation	Mo Kα (graphite monochromated)
linear abs coeff (cm^{-1})	58.05
scan mode	θ–2θ
scan width (deg)	1.0 + 0.35 tan θ
θ limits (deg)	1–25
octants collected	$\pm h$, $+k$, $+l$
data collected	7840
unique data used	5679 ($I > 3\sigma(I)$)
no. of params refined	596
$R_{int} = \sum(F_o^2 - (F_o^2))/\sum F_o^2$	0.04
$R = \sum\|\|F_o\| - \|F_c\|\|/\sum\|F_o\|$	0.042
$R_w = [\sum_w(\|F_o\| - \|F_c\|)^2/\sum_w\|F_o\|^2]^{1/2}$	0.052
GOF = $[\sum_w(\|F_o\| - \|F_c\|)^2/(N_o - N_p)]^{1/2}$	1.52
p fudge factor	0.06
largest shift/esd, final cycle	0.17
largest peak in final diff map (e/Å^3)	0.66

(55) Hoffmann, R. *J. Chem. Phys.* **1963**, *39*, 1397.

The atomic parameters used are summarized in Table V. Idealized experimental molecular structures were considered for isomers a and b and the dimer $[Mo(CO)_3Cp]_2$. In all the calculations, the following bond distances (Å) were used: Pt-Pt = 2.65; Mo-C (Cp) = 2.35; Mo-C (CO) = 1.98; Pt-P = 2.29; C-O = 1.15; C-C = 1.41; P-H = 1.40; and C-H = 1.09.

X-ray Data Collection and Structural Determination for 2b. Single crystals of **2b** were obtained by slow diffusion of *n*-hexane into a CH_2Cl_2 solution of the complex at -20 °C. Crystal data and intensity collection parameters are given in Table VI. Precise lattice parameters were obtained by standard Enraf-Nonius least-squares methods with use of 25 carefully selected reflections and Mo Kα radiation (graphite monochromator, λ = 0.71073 Å). No intensity decay was observed during the data collection periods. Intensity data were collected on an Enraf-Nonius-CAD4 diffractometer, and for all subsequent computations, the Enraf-Nonius SDP package was used.[57] Intensities were corrected for Lorentz and polarization factors except that absorption corrections were omitted. The crystal structures were solved by using the MULTAN program and Fourier methods in the space group $P2_1/n$, assumed on the basis of an $N(z)$ cumulative test on $|F_o|$.[58] Crystal data for $[Pt_2Mo_2Cp'_2(CO)_6(PCy_3)_2]$ (**2b**): $C_{54}H_{80}Mo_2O_6P_2Pt_2$, M_W = 1469.25; monoclinic, $P2_1/n$; crystal dimensions, 0.40 × 0.15 × 0.15 mm; a = 10.321 (3), b = 24.351 (8), c = 21.368 (6) Å; β = 92.76 (4)°; V = 5364 Å^3; Z = 4; $F(000)$ = 2888e; d_{calcd} = 1.819 g·cm^{-3}; 25 °C; μ = 58.05 cm^{-1}; $\pm h$, $+k$, $+l$ octants collected; θ-2θ scan to a maximum θ of 25° and a minimum θ of 1°, giving 7840 unique reflections of which 5679 were used according to the criterion that $I > 3\sigma(I)$. Hydrogen atoms were introduced by their computed coordinates (C-H 0.95 Å) in structure factor calculations with isotropic thermal parameters of 4.0 Å^2 but were not refined. Full least-squares refinements minimizing the function $\sum(|F_o| - |F_c|)^2$ converged to a final $R = \sum||F_o| - |F_c||/\sum|F_o|$ value of 0.042, an $R_w = [\sum_w(|F_o| - |F_c|)^2/\sum_w|F_o|^2]^{1/2}$ value of 0.052 with a (goodness of fit) GOF = $[\sum_w(|F_o| - |F_c|)^2/(\text{number of reflections} - \text{number of parameters})]^{1/2}$ of 1.52. Each reflection was weighted by using $\sigma^2(F_o) = \sigma^2_{counts} + (pI)^2$. A final difference map revealed no significant residual peaks. The neutral atom scattering factors used for all atoms and anomalous dispersion coefficients were obtained from standard sources.[59] Final positional parameters with their estimated standard deviations corresponding to the final least-squares refinement cycles are given in the supplementary material (Table S-I).

Acknowledgment. We are grateful to the CNRS for financial support and to the Johnson Matthey Technology Center for a generous loan of K_2PtCl_4.

Supplementary Material Available: Tables of positional parameters (Table S-I), calculated hydrogen atom coordinates (Table S-II), complete bond lengths and angles (Tables S-III and S-IV), anisotropic thermal parameters (Table S-V) used in the refinement for **2b** (11 pages); listing of the observed and calculated structure factor amplitudes used in the refinement (Table S-VI) for **2b** (29 pages). Ordering information is given on any current masthead page.

(56) Ammeter, J. H.; Bürgi, H. B.; Thibeault, J. C.; Hoffmann, R. *J. Am. Chem. Soc.* **1978**, *100*, 3686.
(57) Frenz, B. A. In *Computing in Crystallography*; Schenk, H., Olthof-Hazekamp, R., van Konigsveld, H., Bassi, G. S., Eds.; University Press: Delft, The Netherlands, 1978; p 64.
(58) Germain, G.; Main, P.; Woolfson, M. M. *Acta Crystallogr.* **1971**, *A27*, 368.
(59) Cromer, D. T.; Waber, J. T. *International Tables for X-Ray Crystallography*; Kynoch Press: Birmingham, England, 1974; Vol. IV, Table 2.

Stereospecificity of the β-Hydroxyl Elimination from the (Hydroxyalkyl)chromium Complex $(H_2O)_5Cr^{III}$-$CH(CH_3)CH(CH_3)OH^{2+}$

Haim Cohen,*[1a,b] Alexander Feldman,[1c] Ruth Ish-Shalom,[1c] and Dan Meyerstein*[1b,c]

Contribution from the Nuclear Research Centre Negev, Beer-Sheva, Israel, and R. Bloch Coal Research Center and Chemistry Department, Ben Gurion University of the Negev, Beer-Sheva, Israel. *Received July 24, 1990*

Abstract: The reaction of the aliphatic free radical $^{\bullet}CH(CH_3)CH(OH)CH_3$ (formed by $^{\bullet}OH$ addition to *cis*-/*trans*-2-butene or by hydrogen abstraction from 2-butanol by $^{\bullet}OH$ free radicals) with chromous ions in aqueous solutions was investigated. The radical reacts with Cr^{2+}(aq), $k = 1.1 \times 10^8$ M^{-1} s^{-1}, to yield a transient complex with a chromium-carbon σ bond. The transient complex decomposes via an acid-catalyzed β-elimination reaction, $k = (230 + 9.8 \times 10^4[H_3O^+])$ s^{-1}, to form a complex in which the tervalent chromium is bound to 2-butene by a d→π bond. This complex decomposes to produce *cis*- or *trans*-2-butene. At pH >2 *cis*- and *trans*-2-butene are produced in equal amounts whereas in acidic solutions, pH <1, the thermodynamically less stable *cis*-2-butene is produced in considerable excess. These results are discussed and tentatively explained by the higher rate of dissociation of the cis d→π complex coupled with an acid-catalyzed isomerization of the two d→π complexes. The rate of the hydrolysis of the chromium d→π complex obeys the rate law $k = (0.8 + 6.7[H_3O^+])$ s^{-1}. The same mechanism also explains the effect of pH on the relative yields of 1-butene and 2-butene obtained in the oxidation of 2-butanol by Cr^{2+}(aq) and H_2O_2. The rates of the β-elimination reactions of $(H_2O)_5Cr^{III}$-$CH_2CH_2OH^{2+}$ and $(H_2O)_5Cr^{III}$-$CH(CH_3)CH_2OH^{2+}$ are also reported; the results indicate that methyl substituents considerably affect the rate of β-elimination reactions.

Introduction

There is a growing interest in the chemistry of complexes with metal-carbon σ bonds in aqueous solutions. This interest stems from the realization that such complexes, which are usually unstable species, play a key role in a variety of important processes. These include the following: (a) biological processes, e.g. reactions catalyzed by vitamin B_{12},[2] oxidations by cytochrome P-450,[3] and reductive desulfurization of a methyl thioether to methane through L^1Ni^{II}-CH_3 (L^1 = tetrahydrocorphin) followed by protonolysis;[4]

(1) (a) Nuclear Research Centre Negev. (b) R. Bloch Coal Research Center, Ben-Gurion University of the Negev. (c) Chemistry Department, Ben-Gurion University of the Negev.

(2) (a) Halpern, J. *Acc. Chem. Res.* **1982**, *15*, 238. (b) Halpern, J. *Pure Appl. Chem.* **1979**, *51*, 2171. (c) Scheffold, R. *Chimia* **1985**, *39*, 203. (d) Halpern, J. *Pure Appl. Chem.* **1983**, *55*, 1059. (e) Babior, B. M. *Acc. Chem. Res.* **1975**, *8*, 376. (f) Abeles, R. H.; Dolphin, D. *Acc. Chem. Res.* **1976**, *9*, 114. (g) Schrauzer, G. N. *Angew. Chem., Int. Ed. Engl.* **1977**, *16*, 233. (h) Finke, R. G.; Schiraldi, D. A.; Mayer, B. *Coord. Chem. Rev.* **1984**, *54*, 1. (i) Bresciani-Pahor, N.; Forlolin, M.; Marzilli, L. G.; Randaccio, L.; Summers, M. F.; Toscano, P. *Coord. Chem. Rev.* **1985**, *63*, 1.
(3) Mansuy, D. *Pure Appl. Chem.* **1987**, *59*, 759.

0002-7863/91/1513-5292$02.50/0